Measurement and interpretation of moments in inclusive semileptonic decays $\bar{B} \to X_c \ell^- \bar{\nu}$

B. Aubert,[1] Y. Karyotakis,[1] J. P. Lees,[1] V. Poireau,[1] E. Prencipe,[1] X. Prudent,[1] V. Tisserand,[1] J. Garra Tico,[2] E. Grauges,[2] M. Martinelli,[3a,3b] A. Palano,[3a,3b] M. Pappagallo,[3a,3b] G. Eigen,[4] B. Stugu,[4] L. Sun,[4] M. Battaglia,[5] D. N. Brown,[5] L. T. Kerth,[5] Yu. G. Kolomensky,[5] G. Lynch,[5] I. L. Osipenkov,[5] K. Tackmann,[5] T. Tanabe,[5] C. M. Hawkes,[6] N. Soni,[6] A. T. Watson,[6] H. Koch,[7] T. Schroeder,[7] D. J. Asgeirsson,[8] B. G. Fulsom,[8] C. Hearty,[8] T. S. Mattison,[8] J. A. McKenna,[8] M. Barrett,[9] A. Khan,[9] A. Randle-Conde,[9] V. E. Blinov,[10] A. D. Bukin,[10,*] A. R. Buzykaev,[10] V. P. Druzhinin,[10] V. B. Golubev,[10] A. P. Onuchin,[10] S. I. Serednyakov,[10] Yu. I. Skovpen,[10] E. P. Solodov,[10] K. Yu. Todyshev,[10] M. Bondioli,[11] S. Curry,[11] I. Eschrich,[11] D. Kirkby,[11] A. J. Lankford,[11] P. Lund,[11] M. Mandelkern,[11] E. C. Martin,[11] D. P. Stoker,[11] S. Abachi,[12] C. Buchanan,[12] H. Atmacan,[13] J. W. Gary,[13] F. Liu,[13] O. Long,[13] G. M. Vitug,[13] Z. Yasin,[13] L. Zhang,[13] V. Sharma,[14] C. Campagnari,[15] T. M. Hong,[15] D. Kovalskyi,[15] M. A. Mazur,[15] J. D. Richman,[15] T. W. Beck,[16] A. M. Eisner,[16] C. A. Heusch,[16] J. Kroseberg,[16] W. S. Lockman,[16] A. J. Martinez,[16] T. Schalk,[16] B. A. Schumm,[16] A. Seiden,[16] L. Wang,[16] L. O. Winstrom,[16] C. H. Cheng,[17] D. A. Doll,[17] B. Echenard,[17] F. Fang,[17] D. G. Hitlin,[17] I. Narsky,[17] T. Piatenko,[17] F. C. Porter,[17] R. Andreassen,[18] G. Mancinelli,[18] B. T. Meadows,[18] K. Mishra,[18] M. D. Sokoloff,[18] P. C. Bloom,[19] W. T. Ford,[19] A. Gaz,[19] J. F. Hirschauer,[19] M. Nagel,[19] U. Nauenberg,[19] J. G. Smith,[19] S. R. Wagner,[19] R. Ayad,[20,†] A. Soffer,[20,‡] W. H. Toki,[20] R. J. Wilson,[20] E. Feltresi,[21] A. Hauke,[21] H. Jasper,[21] T. M. Karbach,[21] J. Merkel,[21] A. Petzold,[21] B. Spaan,[21] K. Wacker,[21] T. Brandt,[22] M. J. Kobel,[22] R. Nogowski,[22] K. R. Schubert,[22] R. Schwierz,[22] J. E. Sundermann,[22,§] A. Volk,[22] D. Bernard,[23] G. R. Bonneaud,[23] E. Latour,[23] M. Verderi,[23] P. J. Clark,[24] S. Playfer,[24] J. E. Watson,[24] M. Andreotti,[25a,25b] D. Bettoni,[25a] C. Bozzi,[25a] R. Calabrese,[25a,25b] A. Cecchi,[25a,25b] G. Cibinetto,[25a,25b] E. Fioravanti,[25a,25b] P. Franchini,[25a,25b] E. Luppi,[25a,25b] M. Munerato,[25a,25b] M. Negrini,[25a,25b] A. Petrella,[25a,25b] L. Piemontese,[25a] V. Santoro,[25a,25b] R. Baldini-Ferroli,[26] A. Calcaterra,[26] R. de Sangro,[26] G. Finocchiaro,[26] S. Pacetti,[26] P. Patteri,[26] I. M. Peruzzi,[26,‖] M. Piccolo,[26] M. Rama,[26] A. Zallo,[26] R. Contri,[27a,27b] E. Guido,[27a] M. Lo Vetere,[27a,27b] M. R. Monge,[27a,27b] S. Passaggio,[27a] C. Patrignani,[27a,27b] E. Robutti,[27a] S. Tosi,[27a,27b] K. S. Chaisanguanthum,[28] M. Morii,[28] A. Adametz,[29] J. Marks,[29] S. Schenk,[29] U. Uwer,[29] F. U. Bernlochner,[30] V. Klose,[30] H. M. Lacker,[30] D. J. Bard,[31] P. D. Dauncey,[31] M. Tibbetts,[31] P. K. Behera,[32] M. J. Charles,[32] U. Mallik,[32] J. Cochran,[33] H. B. Crawley,[33] L. Dong,[33] V. Eyges,[33] W. T. Meyer,[33] S. Prell,[33] E. I. Rosenberg,[33] A. E. Rubin,[33] Y. Y. Gao,[34] A. V. Gritsan,[34] Z. J. Guo,[34] N. Arnaud,[35] J. Béquilleux,[35] A. D'Orazio,[35] M. Davier,[35] D. Derkach,[35] J. Firmino da Costa,[35] G. Grosdidier,[35] F. Le Diberder,[35] V. Lepeltier,[35] A. M. Lutz,[35] B. Malaescu,[35] S. Pruvot,[35] P. Roudeau,[35] M. H. Schune,[35] J. Serrano,[35] V. Sordini,[35,¶] A. Stocchi,[35] G. Wormser,[35] D. J. Lange,[36] D. M. Wright,[36] I. Bingham,[37] J. P. Burke,[37] C. A. Chavez,[37] J. R. Fry,[37] E. Gabathuler,[37] R. Gamet,[37] D. E. Hutchcroft,[37] D. J. Payne,[37] C. Touramanis,[37] A. J. Bevan,[38] C. K. Clarke,[38] F. Di Lodovico,[38] R. Sacco,[38] M. Sigamani,[38] G. Cowan,[39] S. Paramesvaran,[39] A. C. Wren,[39] D. N. Brown,[40] C. L. Davis,[40] A. G. Denig,[41] M. Fritsch,[41] W. Gradl,[41] A. Hafner,[41] K. E. Alwyn,[42] D. Bailey,[42] R. J. Barlow,[42] G. Jackson,[42] G. D. Lafferty,[42] T. J. West,[42] J. I. Yi,[42] J. Anderson,[43] C. Chen,[43] A. Jawahery,[43] D. A. Roberts,[43] G. Simi,[43] J. M. Tuggle,[42] C. Dallapiccola,[44] E. Salvati,[44] S. Saremi,[44] R. Cowan,[45] D. Dujmic,[45] P. H. Fisher,[45] S. W. Henderson,[45] G. Sciolla,[45] M. Spitznagel,[45] R. K. Yamamoto,[45] M. Zhao,[45] P. M. Patel,[46] S. H. Robertson,[46] M. Schram,[46] A. Lazzaro,[47a,47b] V. Lombardo,[47a] F. Palombo,[47a,47b] S. Stracka,[47a,47b] J. M. Bauer,[48] L. Cremaldi,[48] R. Godang,[48,**] R. Kroeger,[48] P. Sonnek,[48] D. J. Summers,[48] H. W. Zhao,[48] M. Simard,[49] P. Taras,[49] H. Nicholson,[50] G. De Nardo,[51a,51b] L. Lista,[51a] D. Monorchio,[51a,51b] G. Onorato,[51a,51b] C. Sciacca,[51a,51b] G. Raven,[52] H. L. Snoek,[52] C. P. Jessop,[53] K. J. Knoepfel,[53] J. M. LoSecco,[53] W. F. Wang,[53] L. A. Corwin,[54] K. Honscheid,[54] H. Kagan,[54] R. Kass,[54] J. P. Morris,[54] A. M. Rahimi,[54] J. J. Regensburger,[54] S. J. Sekula,[54] Q. K. Wong,[54] N. L. Blount,[55] J. Brau,[55] R. Frey,[55] O. Igonkina,[55] J. A. Kolb,[55] M. Lu,[55] R. Rahmat,[55] N. B. Sinev,[55] D. Strom,[55] J. Strube,[55] E. Torrence,[55] G. Castelli,[56a,56b] N. Gagliardi,[56a,56b] M. Margoni,[56a,56b] M. Morandin,[56a] M. Posocco,[56a] M. Rotondo,[56a] F. Simonetto,[56a,56b] R. Stroili,[56a,56b] C. Voci,[56a,56b] P. del Amo Sanchez,[57] E. Ben-Haim,[57] H. Briand,[57] J. Chauveau,[57] O. Hamon,[57] Ph. Leruste,[57] G. Marchiori,[57] J. Ocariz,[57] A. Perez,[57] J. Prendki,[57] S. Sitt,[57] L. Gladney,[58] M. Biasini,[59a,59b] E. Manoni,[59a,59b] C. Angelini,[60a,60b] G. Batignani,[60a,60b] S. Bettarini,[60a,60b] G. Calderini,[60a,60b,††] M. Carpinelli,[60a,60b,‡‡] A. Cervelli,[60a,60b] F. Forti,[60a,60b] M. A. Giorgi,[60a,60b] A. Lusiani,[60a,60c] M. Morganti,[60a,60b] N. Neri,[60a,60b] E. Paoloni,[60a,60b] G. Rizzo,[60a,60b] J. J. Walsh,[60a] D. Lopes Pegna,[61] C. Lu,[61] J. Olsen,[61] A. J. S. Smith,[61] A. V. Telnov,[61] F. Anulli,[62a] E. Baracchini,[62a,62b] G. Cavoto,[62a] R. Faccini,[62a,62b] F. Ferrarotto,[62a] F. Ferroni,[62a,62b] M. Gaspero,[62a,62b] P. D. Jackson,[62a] L. Li Gioi,[62a] M. A. Mazzoni,[62a] S. Morganti,[62a] G. Piredda,[62a] F. Renga,[62a,62b] C. Voena,[62a] M. Ebert,[63] T. Hartmann,[63] H. Schröder,[63] R. Waldi,[63] T. Adye,[64] B. Franek,[64] E. O. Olaiya,[64] F. F. Wilson,[64] S. Emery,[65] L. Esteve,[65] G. Hamel de Monchenault,[65] W. Kozanecki,[65] G. Vasseur,[65] Ch. Yèche,[65]

M. Zito,[65] M. T. Allen,[66] D. Aston,[66] R. Bartoldus,[66] J. F. Benitez,[66] R. Cenci,[66] J. P. Coleman,[66] M. R. Convery,[66] J. C. Dingfelder,[66] J. Dorfan,[66] G. P. Dubois-Felsmann,[66] W. Dunwoodie,[66] R. C. Field,[66] A. M. Gabareen,[66] M. T. Graham,[66] P. Grenier,[66] C. Hast,[66] W. R. Innes,[66] J. Kaminski,[66] M. H. Kelsey,[66] H. Kim,[66] P. Kim,[66] M. L. Kocian,[66] D. W. G. S. Leith,[66] S. Li,[66] B. Lindquist,[66] S. Luitz,[66] V. Luth,[66] H. L. Lynch,[66] D. B. MacFarlane,[66] H. Marsiske,[66] R. Messner,[66,*] D. R. Muller,[66] H. Neal,[66] S. Nelson,[66] C. P. O'Grady,[66] I. Ofte,[66] M. Perl,[66] B. N. Ratcliff,[66] A. Roodman,[66] A. A. Salnikov,[66] R. H. Schindler,[66] J. Schwiening,[66] A. Snyder,[66] D. Su,[66] M. K. Sullivan,[66] K. Suzuki,[66] S. K. Swain,[66] J. M. Thompson,[66] J. Va'vra,[66] A. P. Wagner,[66] M. Weaver,[66] C. A. West,[66] W. J. Wisniewski,[66] M. Wittgen,[66] D. H. Wright,[66] H. W. Wulsin,[66] A. K. Yarritu,[66] K. Yi,[66] C. C. Young,[66] V. Ziegler,[66] X. R. Chen,[67] H. Liu,[67] W. Park,[67] M. V. Purohit,[67] R. M. White,[67] J. R. Wilson,[67] P. R. Burchat,[68] A. J. Edwards,[68] T. S. Miyashita,[68] S. Ahmed,[69] M. S. Alam,[69] J. A. Ernst,[69] B. Pan,[69] M. A. Saeed,[69] S. B. Zain,[69] S. M. Spanier,[70] B. J. Wogsland,[70] R. Eckmann,[71] J. L. Ritchie,[71] A. M. Ruland,[71] C. J. Schilling,[71] R. F. Schwitters,[71] B. C. Wray,[71] B. W. Drummond,[72] J. M. Izen,[72] X. C. Lou,[72] F. Bianchi,[73a,73b] D. Gamba,[73a,73b] M. Pelliccioni,[73a,73b] M. Bomben,[74a,74b] L. Bosisio,[74a,74b] C. Cartaro,[74a,74b] G. Della Ricca,[74a,74b] L. Lanceri,[74a,74b] L. Vitale,[74a,74b] V. Azzolini,[75] N. Lopez-March,[75] F. Martinez-Vidal,[75] D. A. Milanes,[75] A. Oyanguren,[75] J. Albert,[76] Sw. Banerjee,[76] B. Bhuyan,[76] H. H. F. Choi,[76] K. Hamano,[76] G. J. King,[76] R. Kowalewski,[76] M. J. Lewczuk,[76] I. M. Nugent,[76] J. M. Roney,[76] R. J. Sobie,[76] T. J. Gershon,[77] P. F. Harrison,[77] J. Ilic,[77] T. E. Latham,[77] G. B. Mohanty,[77] E. M. T. Puccio,[77] H. R. Band,[78] X. Chen,[78] S. Dasu,[78] K. T. Flood,[78] Y. Pan,[78] R. Prepost,[78] C. O. Vuosalo,[78] and S. L. Wu[78]

[1]*Laboratoire d'Annecy-le-Vieux de Physique des Particules (LAPP), Université de Savoie, CNRS/IN2P3, F-74941 Annecy-Le-Vieux, France*
[2]*Universitat de Barcelona, Facultat de Fisica, Departament ECM, E-08028 Barcelona, Spain*
[3a]*INFN Sezione di Bari, I-70126 Bari, Italy*
[3b]*Dipartimento di Fisica, Università di Bari, I-70126 Bari, Italy*
[4]*University of Bergen, Institute of Physics, N-5007 Bergen, Norway*
[5]*Lawrence Berkeley National Laboratory and University of California, Berkeley, California 94720, USA*
[6]*University of Birmingham, Birmingham, B15 2TT, United Kingdom*
[7]*Ruhr Universität Bochum, Institut für Experimentalphysik 1, D-44780 Bochum, Germany*
[8]*University of British Columbia, Vancouver, British Columbia, Canada V6T 1Z1*
[9]*Brunel University, Uxbridge, Middlesex UB8 3PH, United Kingdom*
[10]*Budker Institute of Nuclear Physics, Novosibirsk 630090, Russia*
[11]*University of California at Irvine, Irvine, California 92697, USA*
[12]*University of California at Los Angeles, Los Angeles, California 90024, USA*
[13]*University of California at Riverside, Riverside, California 92521, USA*
[14]*University of California at San Diego, La Jolla, California 92093, USA*
[15]*University of California at Santa Barbara, Santa Barbara, California 93106, USA*
[16]*University of California at Santa Cruz, Institute for Particle Physics, Santa Cruz, California 95064, USA*
[17]*California Institute of Technology, Pasadena, California 91125, USA*
[18]*University of Cincinnati, Cincinnati, Ohio 45221, USA*
[19]*University of Colorado, Boulder, Colorado 80309, USA*
[20]*Colorado State University, Fort Collins, Colorado 80523, USA*
[21]*Technische Universität Dortmund, Fakultät Physik, D-44221 Dortmund, Germany*
[22]*Technische Universität Dresden, Institut für Kern- und Teilchenphysik, D-01062 Dresden, Germany*
[23]*Laboratoire Leprince-Ringuet, CNRS/IN2P3, Ecole Polytechnique, F-91128 Palaiseau, France*
[24]*University of Edinburgh, Edinburgh EH9 3JZ, United Kingdom*
[25a]*INFN Sezione di Ferrara, I-44100 Ferrara, Italy*
[25b]*Dipartimento di Fisica, Università di Ferrara, I-44100 Ferrara, Italy*
[26]*INFN Laboratori Nazionali di Frascati, I-00044 Frascati, Italy*
[27a]*INFN Sezione di Genova, I-16146 Genova, Italy*
[27b]*Dipartimento di Fisica, Università di Genova, I-16146 Genova, Italy*
[28]*Harvard University, Cambridge, Massachusetts 02138, USA*
[29]*Universität Heidelberg, Physikalisches Institut, Philosophenweg 12, D-69120 Heidelberg, Germany*
[30]*Humboldt-Universität zu Berlin, Institut für Physik, Newtonstr. 15, D-12489 Berlin, Germany*
[31]*Imperial College London, London, SW7 2AZ, United Kingdom*
[32]*University of Iowa, Iowa City, Iowa 52242, USA*
[33]*Iowa State University, Ames, Iowa 50011-3160, USA*
[34]*Johns Hopkins University, Baltimore, Maryland 21218, USA*
[35]*Laboratoire de l'Accélérateur Linéaire, IN2P3/CNRS et Université Paris-Sud 11, Centre Scientifique d'Orsay, B. P. 34, F-91898 Orsay Cedex, France*

[36]*Lawrence Livermore National Laboratory, Livermore, California 94550, USA*

[37]*University of Liverpool, Liverpool L69 7ZE, United Kingdom*

[38]*Queen Mary, University of London, London, E1 4NS, United Kingdom*

[39]*University of London, Royal Holloway and Bedford New College, Egham, Surrey TW20 0EX, United Kingdom*

[40]*University of Louisville, Louisville, Kentucky 40292, USA*

[41]*Johannes Gutenberg-Universität Mainz, Institut für Kernphysik, D-55099 Mainz, Germany*

[42]*University of Manchester, Manchester M13 9PL, United Kingdom*

[43]*University of Maryland, College Park, Maryland 20742, USA*

[44]*University of Massachusetts, Amherst, Massachusetts 01003, USA*

[45]*Massachusetts Institute of Technology, Laboratory for Nuclear Science, Cambridge, Massachusetts 02139, USA*

[46]*McGill University, Montréal, Québec, Canada H3A 2T8*

[47a]*INFN Sezione di Milano, I-20133 Milano, Italy*

[47b]*Dipartimento di Fisica, Università di Milano, I-20133 Milano, Italy*

[48]*University of Mississippi, University, Mississippi 38677, USA*

[49]*Université de Montréal, Physique des Particules, Montréal, Québec, Canada H3C 3J7*

[50]*Mount Holyoke College, South Hadley, Massachusetts 01075, USA*

[51a]*INFN Sezione di Napoli, I-80126 Napoli, Italy*

[51b]*Dipartimento di Scienze Fisiche, Università di Napoli Federico II, I-80126 Napoli, Italy*

[52]*NIKHEF, National Institute for Nuclear Physics and High Energy Physics, NL-1009 DB Amsterdam, The Netherlands*

[53]*University of Notre Dame, Notre Dame, Indiana 46556, USA*

[54]*Ohio State University, Columbus, Ohio 43210, USA*

[55]*University of Oregon, Eugene, Oregon 97403, USA*

[56a]*INFN Sezione di Padova, I-35131 Padova, Italy*

[56b]*Dipartimento di Fisica, Università di Padova, I-35131 Padova, Italy*

[57]*Laboratoire de Physique Nucléaire et de Hautes Energies, IN2P3/CNRS, Université Pierre et Marie Curie-Paris6,
Université Denis Diderot-Paris7, F-75252 Paris, France*

[58]*University of Pennsylvania, Philadelphia, Pennsylvania 19104, USA*

[59a]*INFN Sezione di Perugia, I-06100 Perugia, Italy*

[59b]*Dipartimento di Fisica, Università di Perugia, I-06100 Perugia, Italy*

[60a]*INFN Sezione di Pisa, I-56127 Pisa, Italy*

[60b]*Dipartimento di Fisica, Università di Pisa, I-56127 Pisa, Italy*

[60c]*Scuola Normale Superiore di Pisa, I-56127 Pisa, Italy*

[61]*Princeton University, Princeton, New Jersey 08544, USA*

[62a]*INFN Sezione di Roma, I-00185 Roma, Italy*

[62b]*Dipartimento di Fisica, Università di Roma La Sapienza, I-00185 Roma, Italy*

[63]*Universität Rostock, D-18051 Rostock, Germany*

[64]*Rutherford Appleton Laboratory, Chilton, Didcot, Oxon, OX11 0QX, United Kingdom*

[65]*CEA, Irfu, SPP, Centre de Saclay, F-91191 Gif-sur-Yvette, France*

[66]*SLAC National Accelerator Laboratory, Stanford, California 94309 USA*

[67]*University of South Carolina, Columbia, South Carolina 29208, USA*

[68]*Stanford University, Stanford, California 94305-4060, USA*

[69]*State University of New York, Albany, New York 12222, USA*

[70]*University of Tennessee, Knoxville, Tennessee 37996, USA*

[71]*University of Texas at Austin, Austin, Texas 78712, USA*

[72]*University of Texas at Dallas, Richardson, Texas 75083, USA*

[73a]*INFN Sezione di Torino, I-10125 Torino, Italy*

[73b]*Dipartimento di Fisica Sperimentale, Università di Torino, I-10125 Torino, Italy*

[74a]*INFN Sezione di Trieste, I-34127 Trieste, Italy*

[74b]*Dipartimento di Fisica, Università di Trieste, I-34127 Trieste, Italy*

---

*Deceased

[†]Now at Temple University, Philadelphia, PA 19122, USA

[‡]Now at Tel Aviv University, Tel Aviv, 69978, Israel

[§]Now at Universität Freiburg, D-79104 Freiburg, Germany

[‖]Also with Università di Perugia, Dipartimento di Fisica, Perugia, Italy

[¶]Also with Università di Roma La Sapienza, I-00185 Roma, Italy

[**]Now at University of South AL, Mobile, AL 36688, USA

[††]Also with Laboratoire de Physique Nucléaire et de Hautes Energies, IN2P3/CNRS, Université Pierre et Marie Curie-Paris6,
Université Denis Diderot-Paris7, F-75252 Paris, France

[‡‡]Also with Università di Sassari, Sassari, Italy

[75]*IFIC, Universitat de Valencia-CSIC, E-46071 Valencia, Spain*
[76]*University of Victoria, Victoria, British Columbia, Canada V8W 3P6*
[77]*Department of Physics, University of Warwick, Coventry CV4 7AL, United Kingdom*
[78]*University of Wisconsin, Madison, Wisconsin 53706, USA*

We present results for the moments of observed spectra in inclusive semileptonic B-meson decays to charm hadrons $\bar{B} \to X_c \ell^- \bar{\nu}$. Moments of the hadronic-mass and the combined mass-and-energy spectra for different minimum electron or muon momenta between 0.8 and 1.9 GeV/c are obtained from a sample of 232×10^6 $\Upsilon(4S) \to B\bar{B}$ events, collected with the *BABAR* detector at the PEP-II asymmetric-energy B-meson factory at SLAC. We also present a reevaluation of the moments of electron-energy spectra and partial decay fractions $\mathcal{B}(\bar{B} \to X_c e^- \bar{\nu})$ for minimum electron momenta between 0.6 and 1.5 GeV/c based on a sample of 51×10^6 $\Upsilon(4S) \to B\bar{B}$ events. The measurements are used for the extraction of the total decay fraction, the Cabibbo-Kobayashi-Maskawa (CKM) matrix element $|V_{cb}|$, the quark masses m_b and m_c, and four heavy-quark QCD parameters in the framework of a Heavy-Quark Expansion (HQE). We find $\mathcal{B}(\bar{B} \to X_c \ell^- \bar{\nu}) = (10.64 \pm 0.17 \pm 0.06)\%$ and $|V_{cb}| = (42.05 \pm 0.45 \pm 0.70) \times 10^{-3}$.

I. INTRODUCTION

The standard model of particle physics (SM) contains a large number of free parameters which can only be determined by experiment. Precision measurements of all of these parameters are essential for probing the validity range of the model by comparing many other precision measurements to SM calculations. Three of the parameters, the Cabibbo-Kobayashi-Maskawa (CKM) matrix element $|V_{cb}|$ [1,2] and the heavy-quark masses m_b and m_c, can be related via Operator Product Expansions (OPE) to moments and rates of inclusive distributions in semileptonic B-meson decays, $\bar{B} \to X_c \ell^- \bar{\nu}$ [3], and rare B-meson decays, $\bar{B} \to X_s \gamma$, where X_c and X_s denote the hadronic systems with charm and strangeness in these final states, respectively. The quantities $|V_{cb}|$, m_b, m_c, and nonperturbative parameters describing effects of the strong interaction can be determined from the measured rates and moments using expansions in $1/m_b$ and the strong coupling constant α_s with reliable uncertainty estimates.

Various measurements of moments of the hadronic-mass [4–8] and lepton-energy [7,9,10] spectra in inclusive semileptonic decays $\bar{B} \to X_c \ell^- \bar{\nu}$ have already been used for determinations of $|V_{cb}|$, m_b, m_c, and of four strong-interaction parameters $\mu_\pi^2(\mu)$, $\mu_G^2(\mu)$, $\rho_D^3(\mu)$, and $\rho_{LS}^3(\mu)$. Here, the strong-interaction parameters are defined in the kinetic-mass scheme [11]. The parameters $\mu_\pi^2(\mu)$ and $\mu_G^2(\mu)$ are the expectation values of the kinetic and chromomagnetic dimension-five operators, respectively, and appear at $\mathcal{O}(1/m_b^2)$ in the expansion. The parameters $\rho_D^3(\mu)$ and $\rho_{LS}^3(\mu)$ are the expectation values of the Darwin and spin-orbit dimension-six operators, respectively, and appear at $\mathcal{O}(1/m_b^3)$ in the expansion. Here, μ denotes the Wilson factorization scale that separates effects from long- and short-distance dynamics.

Combined fits to the $\bar{B} \to X_c \ell^- \bar{\nu}$ moments and moments of the photon-energy spectrum in $\bar{B} \to X_s \gamma$ decays [12–16] in the context of Heavy Quark Expansions (HQE) lead to $|V_{cb}| = (41.96 \pm 0.23 \pm 0.69) \times 10^{-3}$ and $m_b = (4.590 \pm 0.025 \pm 0.030)$ GeV/c^2 in the kinetic-mass scheme [17] and $|V_{cb}| = (41.78 \pm 0.30 \pm 0.08) \times 10^{-3}$ and $m_b = (4.701 \pm 0.030)$ GeV/c^2 in the 1S scheme [18]. The Belle Collaboration has presented similar results in [19].

While lepton-energy moments are known with good accuracy, the precision of the hadronic-mass and photon-energy moments is limited by statistics. Therefore, we present a new measurement of the hadronic-mass moments $\langle m_X^k \rangle$ with $k = 1, \ldots, 6$ based on a larger data set than previously used [5]. We also present the first measurement of the combined hadronic mass-and-energy moments $\langle n_X^k \rangle$ with $k = 2, 4, 6$ as proposed by Gambino and Uraltsev [20]. The combined moments $\langle n_X^k \rangle$ use the mass m_X and the energy E_X of the X_c system in the B meson rest frame of $\bar{B} \to X_c \ell^- \bar{\nu}$ decays,

$$n_X^2 = m_X^2 c^4 - 2\tilde{\Lambda} E_X + \tilde{\Lambda}^2, \tag{1}$$

with a constant $\tilde{\Lambda}$, here fixed to be 0.65 GeV as proposed in [20]. They are expected to allow a more reliable extraction of the higher-order nonperturbative HQE parameters and thus to increase the precision on the extraction of $|V_{cb}|$ and the quark masses m_b and m_c. All moments are determined for different values of the minimum energy of the charged lepton.

We update our previous measurement of lepton-energy moments [9] using branching-fraction measurements for background decays in [21] and improving the evaluation of systematic uncertainties.

Finally, we perform a combined fit to the hadronic-mass moments, moments of the lepton-energy spectrum, and moments of the photon-energy spectrum in decays $\bar{B} \to X_s \gamma$. The fit determines $|V_{cb}|$, the quark masses m_b and m_c,

the total semileptonic branching-fraction $\mathcal{B}(\bar{B} \to X_c \ell^- \bar{\nu})$, and the dominant nonperturbative HQE parameters μ_π^2, μ_G^2, ρ_D^3, and ρ_{LS}^3. An alternative fit to the moments of n_X^k, of the lepton-energy, and of the photon energy in $\bar{B} \to X_s \gamma$, leads to essentially the same results.

II. *BABAR* DETECTOR AND DATA SETS

The work is based on data collected with the *BABAR* experiment [22] at the PEP-II asymmetric-energy $e^+ e^-$ storage rings [23] at the SLAC National Accelerator Laboratory.

The *BABAR* tracking system used for charged particle and vertex reconstruction has two main components: a silicon vertex tracker (SVT) and a drift chamber (DCH), both operating within a 1.5T magnetic field of a superconducting solenoid. The transverse momentum resolution is 0.47% at 1 GeV/c. Photons are identified in an electromagnetic calorimeter (EMC) surrounding a detector of internally reflected Cherenkov light (DIRC), which associates Cherenkov photons with tracks for particle identification (PID). The energy of photons is measured with a resolution of 3% at 1 GeV. Muon candidates are identified with the use of the instrumented flux return (IFR) of the solenoid. The tracking system, EMC, and IFR cover the full azimuthal range and the polar-angle range $0.3 < \theta < 2.7$ rad in the laboratory frame, corresponding to a coverage of approximately 90% in the center-of-mass (c.m.) frame, where θ is the polar angle with respect to the electron direction. The DIRC fiducial volume corresponds to a c.m. frame coverage of about 84%.

The data sample for the hadronic moments measurements consists of about 210 fb^{-1}, corresponding to 232 $\times$ 10^6 decays $\Upsilon(4S) \to B\bar{B}$. Our previous measurement of the lepton-energy moments, which is updated in this paper, was based on a data sample of about 51×10^6 $\Upsilon(4S) \to B\bar{B}$ decays. This corresponds to an integrated luminosity of 47 fb^{-1} on the $\Upsilon(4S)$ resonance. In addition, about 9 fb^{-1} of data recorded at an energy 40 MeV below the resonance (off-resonance) was used in the lepton-energy moments measurement for the subtraction of background not originating from the $\Upsilon(4S)$.

We use Monte Carlo (MC) simulated events to determine background distributions and to correct for detector acceptance and resolution effects. Simulated B-meson decays are generated using EvtGen [24]. The simulation of the *BABAR* detector is realized with GEANT4 [25] and final state radiation (FSR) is modeled using the PHOTOS code [26].

In the simulation of semileptonic decays $\bar{B} \to X_c \ell^- \bar{\nu}$ we use the branching fractions listed in Table I. For the dominant decay $\bar{B} \to D^* \ell^- \bar{\nu}$ we use a parametrization of form factors, based on heavy quark effective theory (HQET) [32–34]. Its differential rate is described by three helicity amplitudes which are expressed by the three parameters

TABLE I. Summary of branching fractions of semileptonic decays $\bar{B} \to X_c \ell^- \bar{\nu}$ used in MC simulations for neutral ($\mathcal{B}_{B^0}$) and charged ($\mathcal{B}_{B^\pm}$) B-meson decays. The values are taken from [21,27–30]. Isospin symmetry is assumed to calculate the individual decay rates for B^0 and $B^\pm$ mesons from their averaged measured branching fractions, taking into account the lifetime ratio 1.071 ± 0.009 [21]. The sum of the exclusive decays is constrained to equal the total inclusive branching fractions for $\bar{B} \to X_c \ell^- \bar{\nu}$ decays, $\mathcal{B}(B^+ \to X_c \ell^+ \nu) = 10.89 \pm 0.16$ and $\mathcal{B}(B^0 \to X_c \ell^+ \nu) = 10.15 \pm 0.16$ [27,31].

Semileptonic Decay	$\mathcal{B}_{B^0}$ [%]	$\mathcal{B}_{B^\pm}$ [%]
$\bar{B} \to D \ell^- \bar{\nu}$	2.13 ± 0.14	2.30 ± 0.16
$\bar{B} \to D^* \ell^- \bar{\nu}$	5.53 ± 0.25	5.95 ± 0.24
$\bar{B} \to D_1 \ell^- \bar{\nu}$	0.50 ± 0.08	0.54 ± 0.06
$\bar{B} \to D_2^* \ell^- \bar{\nu}$	0.39 ± 0.07	0.42 ± 0.08
$\bar{B} \to D_0^* \ell^- \bar{\nu}$	0.43 ± 0.09	0.45 ± 0.09
$\bar{B} \to D_1' \ell^- \bar{\nu}$	0.40 ± 0.20	0.45 ± 0.20
$\bar{B} \to D^0 \pi \ell \nu$	0.40 ± 0.12	0.20 ± 0.06
$\bar{B} \to D^\pm \pi \ell \nu$	0.19 ± 0.06	0.40 ± 0.12
$\bar{B} \to D^{*0} \pi \ell \nu$	0.12 ± 0.04	0.06 ± 0.02
$\bar{B} \to D^{*\pm} \pi \ell \nu$	0.06 ± 0.04	0.12 ± 0.04

ρ^2, R_1, and R_2. We choose the central values of the results obtained in [35]: $R_1 = 1.18$, $R_2 = 0.71$, and $\rho^2 = 0.91$. For decays $\bar{B} \to D \ell^- \bar{\nu}$ and for decays to the higher-mass states D_1, D_1', D_0^*, and D_2^* we use the ISGW2 model [36]. For the decays $\bar{B} \to D^{(*)} \pi \ell \bar{\nu}$, we use the prescription by Goity and Roberts [37].

III. RECONSTRUCTION OF SEMILEPTONIC DECAYS FOR THE MEASUREMENT OF HADRONIC MOMENTS

The event selection and reconstruction for the hadronic-mass moments $\langle m_X^k \rangle$ and the combined mass-and-energy moments $\langle n_X^k \rangle$ are almost identical. As described in the corresponding Secs. IV and V, the only differences regard the requirements needed to ensure a good resolution in the observables of interest.

The analysis uses $\Upsilon(4S) \to B\bar{B}$ events in which one of the B mesons decays to hadrons and is fully reconstructed (B_{tag}), and the semileptonic decay of the recoiling $\bar{B}$ meson (B_{recoil}) is identified by the presence of an electron or muon. While this approach results in a low overall event selection efficiency of only a few per mille, it allows for the determination of momentum, charge, and flavor of the B mesons.

A. Selection of hadronic B-meson decays

To obtain a large sample of B_{tag}-mesons, many exclusive hadronic decays $B_{\text{tag}} \to \bar{D}^{(*)} Y^\pm$ are reconstructed [38]. The hadronic system $Y^\pm$ consists of hadrons with a total charge of ± 1. It is composed of $n_\pi \pi^\pm$, $n_K K^\pm$, $n_{K_S^0} K_S^0$, and

$n_{\pi^0}\pi^0$ with $n_\pi + n_K \leq 5$, $n_{K_S^0} \leq 2$, and $n_{\pi^0} \leq 2$, respectively. In total 1097 hadronic decay modes are reconstructed.

The kinematic consistency of the B_{tag} candidates is checked with two variables, the beam-energy-substituted mass $m_{\mathrm{ES}} = \sqrt{s/4 - \vec{p}_B^2}$ and the energy difference $\Delta E = E_B - \sqrt{s}/2$. Here $\sqrt{s}$ is the total energy in the c.m. frame, and $\vec{p}_B$ and E_B denote the c.m. momentum and c.m. energy of the B_{tag} candidate, respectively. The mass m_{ES} is measured with a resolution of 2.5 MeV/c^2, essentially independent of the B_{tag} channel. We require $\Delta E = 0$ within three standard deviations, where one standard deviation ranges between 10 and 30 MeV depending on the number of charged and neutral hadrons in the B_{tag} candidate. For each of the reconstructed hadronic modes the purity is estimated as the fraction of signal decays with $m_{\mathrm{ES}} > 5.27$ GeV/c^2. We restrict the selection to hadronic modes with purities of at least 28% resulting in a selected B_{tag} sample with an overall purity of 60%. On average we reconstruct B_{tag} candidates with an efficiency of about 0.4%.

B. Selection of Semileptonic decays

Semileptonic decays are identified by the presence of one and only one electron or muon above a minimum momentum $p^*_{\ell,\mathrm{min}}$ measured in the rest frame of the B meson. If not stated otherwise, p^*_ℓ will denote in the following the lepton momentum measured in the B-meson rest frame. Electrons are identified by combining information from the EMC, the DCH, and the DIRC. They are required to have a lab-frame momentum of $p > 0.8$ GeV/c and a polar angle in the range $0.41 < \theta < 2.54$ rad. In this range, electrons are selected with 94% average efficiency and a hadron misidentification rate of the order of 0.1%. Muon identification is mainly based on information obtained from the IFR. Muons are identified with an efficiency ranging between 60% for momenta $p = 1$ GeV/c in the laboratory frame and 75% for momenta $p > 2$ GeV/c. The misidentification rate ranges between 1% for kaons and protons and 3% for pions. Efficiencies and misidentification rates are estimated from control samples of electrons, muons, pions, and kaons. We impose the condition $Q_b Q_\ell < 0$, where Q_ℓ is the charge of the lepton and Q_b is the charge of the b quark of the B_{tag}. This condition is fulfilled for primary leptons originating directly from the B decay, except for $B^0\bar{B}^0$ events in which flavor mixing has occurred. We require the total observed charge of the event to be $|Q_{\mathrm{tot}}| = |Q_{B_{\mathrm{tag}}} + Q_{B_{\mathrm{recoil}}}| \leq 1$, allowing for a charge imbalance in events with low momentum tracks or photon conversions. In cases where only one charged track is present in the reconstructed X_c system, the total charge in the event is required to be zero.

C. Reconstruction of the hadronic system

The hadronic system X_c in the decay $\bar{B} \rightarrow X_c \ell^- \bar{\nu}$ is reconstructed from charged tracks and energy deposits in the calorimeter that are not associated to the B_{tag} or the charged lepton. We ignore tracks and energy deposits in the calorimeter which are compatible with the hypothesis of being reconstruction artifacts, low-energy beam-generated photons or calorimeter deposits originating from hadronic showers. Each track is assigned a specific particle type, either $\overset{(-)}{p}$, $K^\pm$, or $\pi^\pm$, based on combined information from the different *BABAR* subdetectors. Few events containing single protons are kept in the selection but removed later on in the background removal procedure. The four-momentum P_{X_c} of the reconstructed hadronic system is obtained from the four-momenta of the reconstructed tracks $P_{i,\mathrm{trk}}$ for the given mass assignment, and photons $P_{i,\gamma}$ by $P_{X_c} = \sum_{i=1}^{N_{\mathrm{trk}}} P_{i,\mathrm{trk}} + \sum_{i=1}^{N_\gamma} P_{i,\gamma}$. The hadronic mass is defined by $m_X^2 = P_{X_c}^2$.

The four-momentum of the unmeasured neutrino is calculated from the missing four-momentum $P_{\mathrm{miss}} = P_{\Upsilon(4S)} - P_{B_{\mathrm{tag}}} - P_{X_c} - P_\ell$. Here, all four-momenta are measured in the laboratory frame. To ensure a well reconstructed hadronic system, we impose criteria on the missing energy, $E_{\mathrm{miss}} > 0.5$ GeV, the missing momentum, $p_{\mathrm{miss}} > 0.5$ GeV/c, and the difference of both quantities, $|E_{\mathrm{miss}} - c p_{\mathrm{miss}}| < 0.5$ GeV.

We perform a kinematic fit exploiting the fact that B mesons are produced in a well-defined initial state $e^+ e^- \rightarrow \Upsilon(4S) \rightarrow B\bar{B}$, to improve the resolution and reduce the bias on the reconstructed quantities. The fit imposes four-momentum conservation, the equality of the masses of the two B mesons, and constrains the mass of the neutrino, $P_{\mathrm{miss}}^2 = 0$. The resulting (original) average resolutions on the measurement of m_X and n_X^2 are 0.355 GeV/c^2 (0.425 GeV/c^2) and 1.05 GeV^2 (1.17 GeV^2), respectively. The average biases of m_X and n_X^2 after (before) the kinematic fit are found to be -0.096 GeV/c^2 (-0.254 GeV/c^2) and -0.11 GeV^2 (-0.37 GeV^2), respectively.

The background is composed of $e^+ e^- \rightarrow q\bar{q}(q = u, d, s, c)$ events (continuum background), $\Upsilon(4S) \rightarrow B^+B^-$ or $B^0\bar{B}^0$ decays in which the B_{tag} candidate is mistakenly reconstructed from particles coming from both B mesons in the event (combinatorial background), and nonsignal decays of the recoiling B_{recoil} meson (residual background). Signal events where the hadronic system is not fully reconstructed are not considered as an additional source of background. The effect of missing tracks and photons on the resolution of the kinematical quantities of interest is taken into account by applying the correction procedures described below.

To quantify the amount of continuum and combinatorial background in the m_{ES} signal region we perform a fit to the m_{ES} distribution of the B_{tag} candidates. We parametrize the
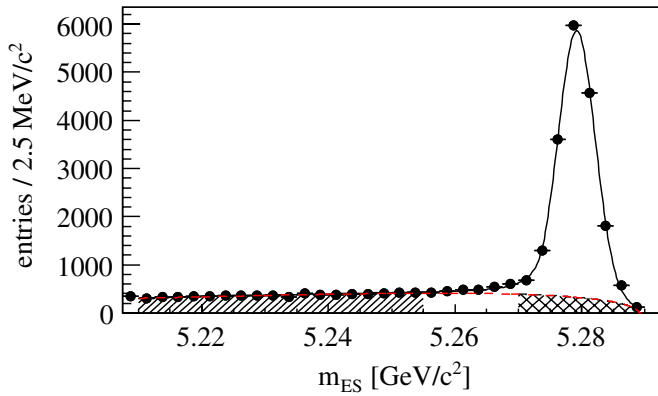
FIG. 1 (color online). The m_{ES} spectrum of B_{tag} decays accompanied by a lepton with $p_\ell^* \geq 0.8$ GeV/c. The fit functions for the sum of signal and background (solid line) and the background (red dashed line) are overlaid. The crossed area shows the predicted background under the B_{tag} signal. The background control region in the m_{ES} sideband is indicated by the hatched area.

background using an empirical threshold function [39],

$$\frac{dN}{dm_{\text{ES}}} \propto m_{\text{ES}}\sqrt{1 - x^2}\, e^{-\chi(1-x^2)}, \qquad (2)$$

where $x = m_{\text{ES}}/m_{\text{ES,max}}$, $m_{\text{ES,max}} = 5.289$ GeV/c^2 is the kinematic endpoint approximated by the mean c.m. energy, and χ is a free parameter defining the curvature of the function. The signal is parametrized with a modified Gaussian function [40] peaked at the B-meson mass and corrected for radiation losses. The fit is performed separately for several bins in m_X and n_X^2 to account for changing background contributions. Figure 1 shows the m_{ES} distribution for $p_\ell^* \geq 0.8$ GeV/c together with the fitted signal and background contributions. The shape of the continuum and combinatorial background as function of m_X and n_X^2 is determined in a signal-free region of the m_{ES} sideband, $5.210 \leq m_{\text{ES}} \leq 5.255$ GeV/c^2. Its overall size in the m_{ES} signal region, $m_{\text{ES}} > 5.27$ GeV/c^2, is determined by re-scaling with the relative background contributions in the signal and sideband regions as determined by the fit. Signal and sideband region are separated by 15 MeV/c^2 to avoid the leakage of signal events into the sideband region.

Residual background is estimated from MC simulations. It is composed of charmless semileptonic decays $\bar{B} \to X_u \ell^- \bar{\nu}$, hadrons misidentified as leptons, secondary leptons from semileptonic decays of $D^{(*)}$, D_s^+ mesons or τ either in $B^0\bar{B}^0$ mixed events or produced in $b \to c\bar{c}s$ transitions, as well as leptons from decays of J/ψ and $\psi(2S)$. In addition, the residual background estimation accounts for B_{tag} mesons reconstructed with the wrong charge or b quark flavor. The branching fractions of the individual simulated background decays are scaled to agree with measurements [21,27,41,42]. The overall simulated background spectrum is normalized to the number of

B_{tag} events in data. We verify the normalization and the shape using an independent data control sample with inverted lepton charge correlation, $Q_b Q_\ell > 0$.

IV. HADRONIC-MASS MOMENTS

We present measurements of the moments $\langle m_X^k \rangle$, with $k = 1, \ldots 6$, of the hadronic-mass distribution in semileptonic B-meson decays $\bar{B} \to X_c \ell^- \bar{\nu}$. The moments are measured as functions of the lower limit on the lepton-momentum $p_{\ell,\text{min}}^*$ between 0.8 GeV/c and 1.9 GeV/c, calculated in the rest frame of the B meson.

A. Selected event sample

We find 19 212 events with $p_\ell^* \geq 0.8$ GeV/c, composed of 15 085 ± 146 signal events above a combinatorial and continuum background of 2429 ± 43 events and residual background of 1696 ± 19 events. Signal decays amount to 79% of the selected event sample. For $p_\ell^* \geq 1.9$ GeV/c, we find in total 2527 events composed of 2006 ± 53 signal events above a background of 271 ± 17 and 248 ± 7 combinatorial/continuum and residual events, respectively. Figure 2 shows the m_X distributions after the kinematic
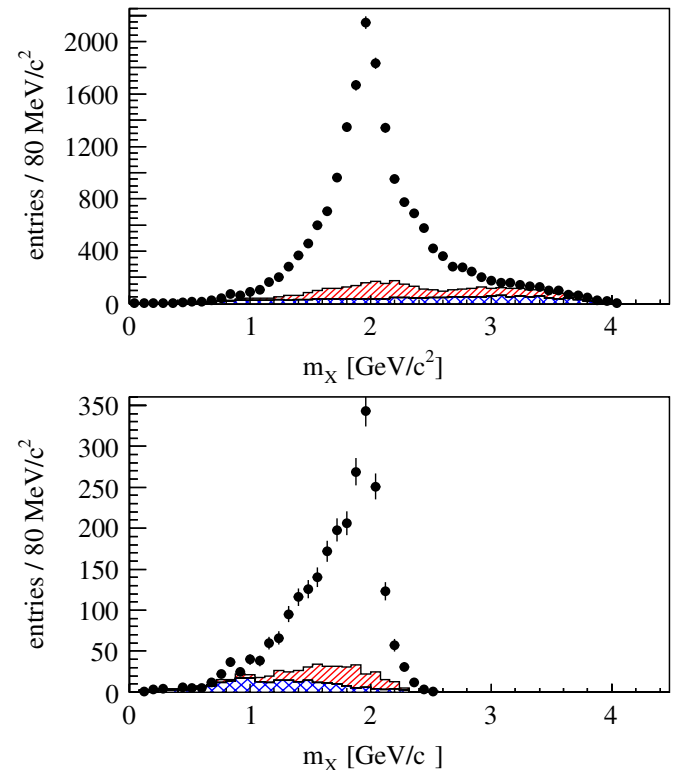

FIG. 2 (color online). Hadronic-mass spectra after the kinematic fit for lepton momenta $p_\ell^* \geq 0.8$ GeV/c (top) and $p_\ell^* \geq 1.9$ GeV/c (bottom) together with distributions of combinatorial background and background from non-$B\bar{B}$ decays (red, hatched area) as well as residual background (blue, crossed area). The two background histograms are plotted on top of each other.

fit together with the extracted background shapes for $p_\ell^* \geq 0.8$ GeV/c and $p_\ell^* \geq 1.9$ GeV/c.

B. Extraction of moments

To extract unbiased moments $\langle m_X^k \rangle$, we apply corrections to account for effects that distort the measured m_X distribution. Contributing effects are the limited acceptance and resolution of the *BABAR* detector resulting in unmeasured particles and in misreconstructed energies and momenta of particles. In addition, there are contributions from measured particles not belonging to the hadronic system, especially photons originating from FSR of the primary leptons. These photons are included in the measured X_c system and thus lead to a modified value of its mass; they also lower the momentum of the primary lepton. Both effects are included in our correction procedure.

We correct the kinematically-fitted value of m_X^k of each event by applying correction factors on an event-by-event basis using the observed linear relationship between the moments of the measured mass $\langle m_{X,\mathrm{reco}}^k \rangle$ and the moments of the true mass $\langle m_{X,\mathrm{true}}^k \rangle$ in MC spectra. The correction factors are determined from MC simulations by calculating moments $\langle m_{X,\mathrm{reco}}^k \rangle$ and $\langle m_{X,\mathrm{true}}^k \rangle$ in several bins of the true mass $m_{X,\mathrm{true}}$ and fitting the observed dependence with a linear function, referred to as calibration function in the following.

We find that the bias of the measured moments $\langle m_{X,\mathrm{reco}}^k \rangle$ is not constant over the whole phase space. Therefore, we derive the calibration functions in three bins of the particle multiplicity N_{X_c} in the X_c system, three bins of $E_{\mathrm{miss}} - cp_{\mathrm{miss}}$, as well as in 12 bins of p_ℓ^*, each with a width of 100 MeV/c. Because of the limited number of generated MC events, the binning in N_{X_c} and $E_{\mathrm{miss}} - cp_{\mathrm{miss}}$ is not used for $p_{\ell,\mathrm{min}}^* \geq 1.7$ GeV/c. Overall we construct 84 calibration functions for each order of moments. The obtained calibration functions allow a consistent extraction of moments for events containing an electron or a muon. Figure 3 shows examples of calibration functions for the moment $\langle m_X^2 \rangle$ in three bins of p_ℓ^* as well as in nine bins of $E_{\mathrm{miss}} - cp_{\mathrm{miss}}$ and N_{X_c}.

For each data event i, the corrected mass $m_{X,\mathrm{calib},i}^k$ is calculated by inverting the linear function,

$$m_{X,\mathrm{calib},i}^k = \frac{m_{X,\mathrm{reco},i}^k - A(E_{\mathrm{miss}} - cp_{\mathrm{miss}}, N_{X_c}, k, p_\ell^*)}{B(E_{\mathrm{miss}} - cp_{\mathrm{miss}}, N_{X_c}, k, p_\ell^*)}, \quad (3)$$

where A is the offset and B is the slope of the calibration function. Background contributions are removed by applying a weight factor w_i to each corrected hadronic-mass $m_{X,\mathrm{calib},i}^k$, where the weight is the expected fraction of signal events in the corresponding region of the $m_{X,\mathrm{reco}}$ spectrum in Fig. 2. The expression used to calculate the moments is the following:

$$\langle m_X^k \rangle = \frac{\sum_{i=1}^{N_{\mathrm{ev}}} w_i(m_X) m_{X,\mathrm{calib},i}^k}{\sum_i^{N_{\mathrm{ev}}} w_i} \times \mathcal{C}_{\mathrm{cal}}(p_\ell^*, k) \times \mathcal{C}_{\mathrm{true}}(p_\ell^*, k), \quad (4)$$

with N_{ev} the total number of selected events. The factors $\mathcal{C}_{\mathrm{cal}}$ and $\mathcal{C}_{\mathrm{true}}$ depend on the order k and the minimum lepton-momentum $p_{\ell,\mathrm{min}}^*$ of the measured moment. They are determined in MC simulations and correct for the residual small biases observed after the calibration. The factors $\mathcal{C}_{\mathrm{cal}}$ account for the bias of the applied correction method and are typically ranging between 1.01 and 1.06 for $k = 1 \ldots 5$. Larger bias corrections $\mathcal{C}_{\mathrm{cal}}$ are observed for $\langle m_X^6 \rangle$ ranging between the extremes 0.902 and 1.109. The residual bias-correction factor $\mathcal{C}_{\mathrm{true}}$ accounts for differences in selection efficiencies for different hadronic final states and FSR that is included in the measured hadron mass and distorts the measurement of the lepton's momentum. Our correction procedure results in moments which are within systematic uncertainties free of photon radiation. The correction $\mathcal{C}_{\mathrm{true}}$ is estimated in MC simulations and typically ranges between 0.994 and 1.007. For the moments $\langle m_X^5 \rangle$ and $\langle m_X^6 \rangle$, slightly higher correction factors are determined, ranging between 0.990 and 1.014 for $\langle m_X^5 \rangle$ and 0.986 and 1.024 for $\langle m_X^6 \rangle$.

This correction procedure is verified on a MC sample by applying the calibration to measured hadron masses of individual semileptonic decays, $\bar{B} \to D\ell^-\bar{\nu}$, $\bar{B} \to D^*\ell^-\bar{\nu}$, four resonant decays $\bar{B} \to D^{**}\ell\bar{\nu}$, and two non-resonant decays $\bar{B} \to D^{(*)}\pi\ell\bar{\nu}$. Figure 4 shows the corrected moments $\langle m_X^2 \rangle$ and $\langle m_X^4 \rangle$ as functions of the true moments for minimum lepton momenta $p_\ell^* \geq 0.8$ GeV/c. The dashed line corresponds to $\langle m_{X,\mathrm{calib}}^k \rangle = \langle m_{X,\mathrm{true}}^k \rangle$. The calibration reproduces the true moments over the full mass range.

C. Systematic uncertainties and tests

The main systematic uncertainties are associated with the modeling of hadronic final states in semileptonic B-meson decays, the bias of the calibration method, the determination of residual background contributions, the modeling of track and photon selection efficiencies, and the identification of particles. The total systematic uncertainty is estimated by adding in quadrature five contributions, as described below. Tables II and III list the individual contributions to the systematic errors of the measured moments $\langle m_X^k \rangle$ with $k = 1 \ldots 6$ for minimum lepton momenta ranging from 0.8 to 1.9 GeV/c.

1. MC statistics

The effect of limited MC statistics on the extracted moments is evaluated using parametrized MC experiments. To study the effect on the calibration curves, the parameters of the fitted first-order polynomials are randomly
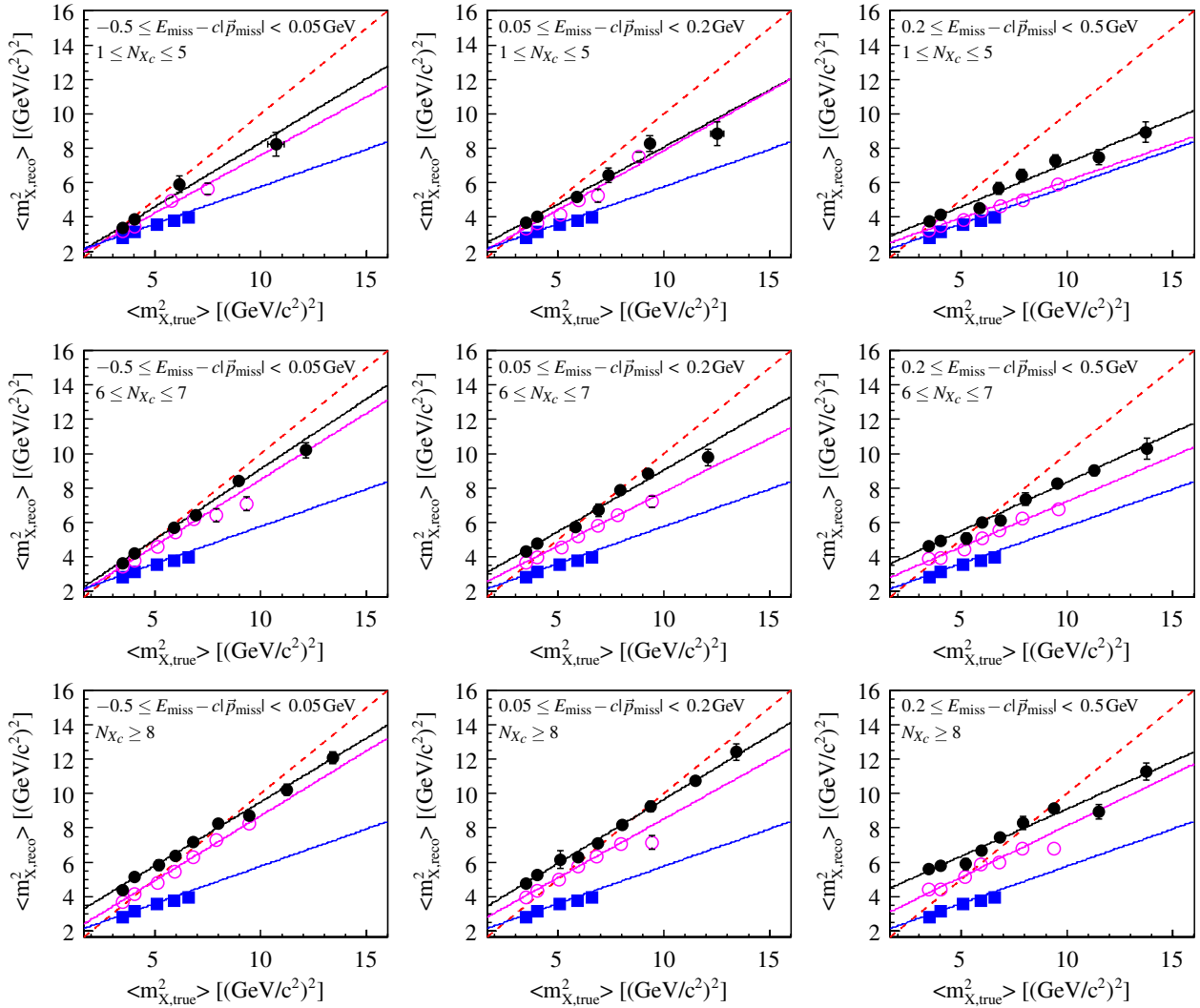
FIG. 3 (color online). Examples of calibration functions for $\langle m_X^2 \rangle$ in bins of N_{X_c}, $E_{\mathrm{miss}} - cp_{\mathrm{miss}}$ and p_ℓ^*. Shown are the extracted moments $\langle m_{X,\mathrm{reco}}^2 \rangle$ versus the true moments $\langle m_{X,\mathrm{true}}^2 \rangle$ for $0.8 \leq p_\ell^* < 0.9$ GeV/c (●), $1.4 \leq p_\ell^* < 1.5$ GeV/c (○), and $p_\ell^* \geq 1.9$ GeV/c (■). The results of fits of linear functions are overlaid as solid lines. A reference line with $\langle m_{X,\mathrm{reco}}^2 \rangle = \langle m_{X,\mathrm{true}}^2 \rangle$ is superimposed (dashed line). The calibration function for $p_\ell^* \geq 1.9$ GeV/c is constructed independent of N_{X_c} and $E_{\mathrm{miss}} - cp_{\mathrm{miss}}$. It is plotted in each of the bins for comparison only.
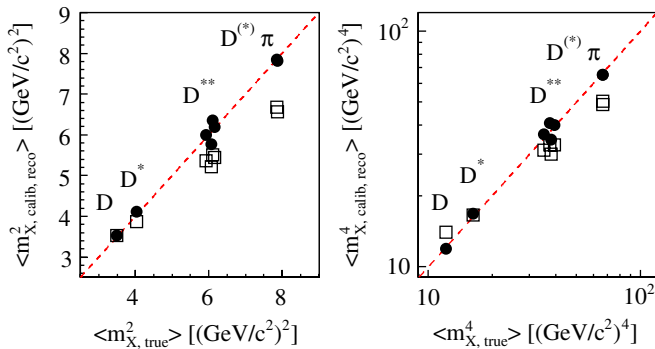

FIG. 4 (color online). Calibrated (●) and uncorrected (□) moments $\langle m_X^2 \rangle$ (left) and $\langle m_X^4 \rangle$ (right) of individual hadronic modes for lepton momenta $p_\ell^* \geq 0.8$ GeV/c. A reference line with $\langle m_{X,\mathrm{calib}} \rangle = \langle m_{X,\mathrm{true}} \rangle$ is superimposed.

varied within their uncertainties including correlations and new sets of moments are extracted. The overall uncertainty is determined by repeating this procedure 250 times and taking the r.m.s. of the distribution of the moments as the systematic uncertainty.

To estimate the effect of limited MC statistics in the residual background determination a similar method is applied by varying the parameters of the fit to the m_{ES} distribution within their errors including correlations.

2. Simulation-related effects

We correct for differences between data and MC simulation in the selection efficiencies of charged tracks and photons, as well as identification efficiencies and misidentification rates of various particle types. The corrections are extracted from data and MC control samples.

TABLE II. Results for the moments $\langle m_X^k \rangle$ with $k = 1 \ldots 3$ for different minimum lepton momenta $p_{\ell,\min}^*$ with statistical and systematic uncertainties. The systematic uncertainties are grouped in five categories having related sources: *MC statistics* contains the statistical uncertainties of the calibration curves and of the residual background. *Simulation related* is the sum of uncertainties due to neutral and charged reconstruction efficiency differences in data and MC, particle identification, and mismodeling of final state radiation. The category *extraction method* contains the conservative estimate of half of the bias correction. The category *background* sums all contributions from the variation of the residual background components. The category *signal model* sums the impact of the variation of the signal decay branching fractions. Minimum lepton momenta are given in GeV/c. Moments and uncertainties are given in (GeV/c^2)^k.

k	$p_{\ell,\min}^*$ [GeV/c]	$\langle m_X^k \rangle$	σ_{stat}	σ_{sys}	MC statistics	simulation related	extraction method	background	signal model
1	0.8	2.0906	±0.0063	±0.0166	0.0058	0.0099	0.0096	0.0047	0.0031
	0.9	2.0890	±0.0062	±0.0158	0.0048	0.0088	0.0103	0.0045	0.0028
	1.0	2.0843	±0.0061	±0.0153	0.0044	0.0076	0.0109	0.0044	0.0027
	1.1	2.0765	±0.0063	±0.0165	0.0044	0.0072	0.0127	0.0047	0.0026
	1.2	2.0671	±0.0064	±0.0160	0.0046	0.0073	0.0120	0.0045	0.0025
	1.3	2.0622	±0.0068	±0.0168	0.0048	0.0073	0.0131	0.0050	0.0023
	1.4	2.0566	±0.0073	±0.0183	0.0047	0.0069	0.0150	0.0054	0.0021
	1.5	2.0494	±0.0081	±0.0198	0.0036	0.0074	0.0168	0.0061	0.0019
	1.6	2.0430	±0.0092	±0.0221	0.0038	0.0082	0.0187	0.0070	0.0018
	1.7	2.0387	±0.0109	±0.0265	0.0047	0.0081	0.0232	0.0083	0.0015
	1.8	2.0370	±0.0143	±0.0337	0.0069	0.0097	0.0299	0.0098	0.0013
	1.9	2.0388	±0.0198	±0.0413	0.0082	0.0123	0.0355	0.0150	0.0008
2	0.8	4.429	±0.029	±0.070	0.027	0.047	0.030	0.018	0.008
	0.9	4.416	±0.027	±0.063	0.020	0.041	0.033	0.016	0.008
	1.0	4.394	±0.026	±0.058	0.020	0.033	0.035	0.015	0.008
	1.1	4.354	±0.026	±0.063	0.019	0.031	0.043	0.016	0.008
	1.2	4.308	±0.026	±0.058	0.019	0.030	0.039	0.015	0.007
	1.3	4.281	±0.027	±0.061	0.020	0.029	0.044	0.016	0.007
	1.4	4.253	±0.028	±0.066	0.021	0.028	0.051	0.018	0.006
	1.5	4.220	±0.031	±0.070	0.015	0.029	0.058	0.019	0.006
	1.6	4.183	±0.034	±0.078	0.015	0.032	0.065	0.022	0.005
	1.7	4.158	±0.040	±0.094	0.019	0.032	0.082	0.026	0.004
	1.8	4.145	±0.051	±0.120	0.026	0.036	0.107	0.031	0.004
	1.9	4.136	±0.069	±0.142	0.031	0.046	0.122	0.048	0.002
3	0.8	9.57	±0.11	±0.25	0.11	0.18	0.07	0.06	0.02
	0.9	9.49	±0.10	±0.22	0.08	0.15	0.08	0.05	0.03
	1.0	9.41	±0.09	±0.18	0.06	0.11	0.09	0.04	0.03
	1.1	9.25	±0.09	±0.19	0.06	0.10	0.11	0.04	0.03
	1.2	9.09	±0.08	±0.18	0.06	0.10	0.10	0.04	0.02
	1.3	8.98	±0.08	±0.18	0.06	0.09	0.11	0.04	0.02
	1.4	8.88	±0.09	±0.19	0.06	0.09	0.13	0.04	0.02
	1.5	8.75	±0.09	±0.19	0.04	0.09	0.15	0.05	0.02
	1.6	8.61	±0.10	±0.22	0.05	0.10	0.17	0.06	0.02
	1.7	8.51	±0.11	±0.26	0.05	0.10	0.22	0.07	0.01
	1.8	8.45	±0.14	±0.33	0.07	0.11	0.29	0.08	0.01
	1.9	8.38	±0.19	±0.38	0.08	0.13	0.32	0.12	0.00

The systematic uncertainties of the photon selection and track finding efficiencies are determined studying independent control samples. Their impact on the measured moments has been evaluated by randomly excluding neutral or charged candidates from the X_c system with probabilities corresponding to the uncertainties of the efficiency extraction methods. The uncertainty of the photon selection efficiencies is found to be 1.8% per photon independent of energy, polar angle, and multiplicity. The uncertainty in

track finding efficiencies consists of two parts. For each track, we add in quadrature 0.8% systematic uncertainty and the statistical uncertainty of the control samples that depend on energy and polar angle of the track as well as the multiplicity of tracks in the reconstructed event.

The systematic uncertainty on the misidentification of $\pi^\pm$ mesons as leptons is found to affect the overall normalization of the corresponding background spectra by 8%. The influence on the measured moments is estimated

TABLE III.   Results for the moments $\langle m_X^k \rangle$ with $k = 4 \ldots 6$ for different minimum lepton momenta $p_{\ell,\min}^*$ with statistical and systematic uncertainties. The systematic uncertainties are grouped in five categories having related sources: *MC statistics* contains the statistical uncertainties of the calibration curves and of the residual background. *Simulation related* is the sum of uncertainties due to neutral and charged reconstruction efficiency differences in data and MC, particle identification, and mismodeling of final state radiation. The category *extraction method* contains the conservative estimate of half of the bias correction. The category *background* sums all contributions from the variation of the residual background components. The category *signal model* sums the impact of the variation of the signal decay branching fractions. moment measurements. Minimum lepton momenta are given in GeV/c. Moments and uncertainties are given in $(\text{GeV}/c^2)^k$.

k	$p_{\ell,\min}^*$ [GeV/c]	$\langle m_X^k \rangle$	σ_{stat}	σ_{sys}	MC statistics	simulation related	extraction method	background	signal model
4	0.8	21.20	±0.39	±0.84	0.35	0.61	0.14	0.19	0.11
	0.9	20.83	±0.33	±0.69	0.26	0.51	0.17	0.15	0.11
	1.0	20.55	±0.30	±0.56	0.24	0.35	0.19	0.12	0.12
	1.1	20.01	±0.27	±0.55	0.19	0.32	0.27	0.11	0.12
	1.2	19.48	±0.25	±0.49	0.17	0.29	0.23	0.09	0.10
	1.3	19.09	±0.25	±0.52	0.17	0.33	0.27	0.10	0.07
	1.4	18.77	±0.25	±0.52	0.17	0.29	0.32	0.11	0.07
	1.5	18.33	±0.26	±0.50	0.13	0.24	0.37	0.11	0.06
	1.6	17.85	±0.27	±0.55	0.12	0.27	0.42	0.13	0.05
	1.7	17.50	±0.30	±0.66	0.14	0.26	0.56	0.15	0.03
	1.8	17.28	±0.37	±0.83	0.18	0.27	0.73	0.18	0.03
	1.9	16.99	±0.48	±0.90	0.21	0.34	0.76	0.27	0.01
5	0.8	48.51	±1.39	±2.90	1.37	2.10	0.15	0.64	0.51
	0.9	46.87	±1.14	±2.21	0.84	1.67	0.31	0.46	0.49
	1.0	46.00	±0.97	±1.74	0.79	1.07	0.36	0.32	0.50
	1.1	44.20	±0.85	±1.61	0.57	0.94	0.60	0.30	0.48
	1.2	42.55	±0.77	±1.44	0.53	0.88	0.50	0.24	0.37
	1.3	41.29	±0.72	±1.47	0.43	1.01	0.61	0.24	0.28
	1.4	40.31	±0.70	±1.45	0.47	0.94	0.74	0.25	0.26
	1.5	38.88	±0.70	±1.26	0.33	0.65	0.84	0.26	0.23
	1.6	37.35	±0.70	±1.38	0.34	0.71	1.00	0.29	0.15
	1.7	36.28	±0.78	±1.61	0.34	0.68	1.32	0.34	0.10
	1.8	35.56	±0.94	±2.00	0.47	0.69	1.73	0.41	0.08
	1.9	34.58	±1.18	±2.11	0.56	0.86	1.73	0.61	0.04
6	0.8	115.20	±4.73	±11.43	4.39	6.84	5.64	2.02	3.76
	0.9	107.97	±3.74	±8.32	2.54	5.36	3.74	1.36	3.22
	1.0	105.19	±3.09	±6.19	2.34	3.27	2.26	0.87	3.05
	1.1	99.35	±2.60	±5.19	1.90	2.85	0.81	0.79	2.80
	1.2	94.82	±2.28	±4.35	1.53	2.49	0.23	0.57	2.16
	1.3	91.01	±2.05	±4.09	1.36	2.73	0.31	0.53	1.73
	1.4	88.02	±1.94	±3.86	1.23	2.57	0.94	0.53	1.57
	1.5	83.46	±1.86	±3.35	0.88	2.20	1.07	0.53	1.47
	1.6	78.84	±1.81	±3.17	0.84	1.85	1.73	0.61	0.97
	1.7	75.87	±1.98	±3.92	0.91	1.73	3.10	0.76	0.29
	1.8	73.66	±2.35	±4.70	1.06	1.69	4.05	0.91	0.25
	1.9	70.70	±2.83	±4.77	1.23	2.09	3.86	1.33	0.14

by varying the corresponding background within its uncertainty. The observed variation of moments is taken as a systematic uncertainty.

The impact of mismodeling FSR simulated with PHOTOS [26] is estimated by calculating moments from data using a set of calibration curves constructed from events simulated without FSR photons. The theoretical uncertainty associated with the calculations included in

PHOTOS is conservatively assumed to be of the order of 20%. The systematic uncertainty connected to the mismodeling of FSR photons is therefore estimated to be 20% of the observed difference between the nominal moments and those from the MC simulation without FSR photons.

A significant fraction of the low-energy photons detected in the calorimeter are beam related. We check the impact of low-energy photons by removing EMC signals

with energies below 100 MeV from the reconstructed hadronic system. The effect on the measured moments is found to be negligible.

The stability of the result under variation of the selection criteria on $E_{\rm miss} - cp_{\rm miss}$ is tested by varying the applied cut between $|E_{\rm miss} - cp_{\rm miss}| < 0.2$ GeV and $|E_{\rm miss} - cp_{\rm miss}| < 1.4$ GeV. For all measured moments, the observed variation is well covered by other known systematic detector and MC simulation effects. Therefore, no contribution is added to the systematic uncertainty.

3. Extraction method

The systematic uncertainty of the calibration bias correction $\mathcal{C}_{\rm cal}$ is estimated to be $(\mathcal{C}_{\rm cal} - 1)/2$.

4. Background determination

The branching fractions of background decays in the MC simulation are scaled to agree with the current measurements [21,27,41,42]. The associated systematic uncertainty is estimated by varying these branching fractions within their uncertainties. At low $p^*_{\ell,\rm min}$, most of the studied background channels contribute to the systematic uncertainty equally, while at high $p^*_{\ell,\rm min}$, the systematic uncertainty is dominated by background from decays $\bar{B} \to X_u \ell^- \bar{\nu}$. Contributions from J/ψ and $\psi(2S)$ decays are found to be negligible.

The uncertainty in the combinatorial $B_{\rm tag}$ background determination is estimated by varying the lower and upper limits of the sideband region in the $m_{\rm ES}$ distribution up and down by 2.5 MeV/c^2. The observed effect on all hadronic-mass moments is found to be negligible.

5. Modeling of signal decays

The uncertainty of the calibration method with respect to the chosen signal model is estimated by changing the composition of the simulated inclusive hadronic spectrum. The dependence on the simulation of high mass hadronic final states is estimated by constructing calibration functions only from MC simulated hadronic events with hadronic masses $m_{X,\rm true} < 2.5$ GeV/c^2, thereby removing the high mass tail of the simulated hadronic-mass spectrum. The model dependence of the calibration method is found to be a small contribution to the total systematic uncertainty.

We estimate the model dependence of the residual bias-correction $\mathcal{C}_{\rm true}$ by changing the composition of the inclusive hadronic spectrum, i.e. omitting one or more decay modes.

We study the effect of differences between data and MC simulation in the multiplicity and $E_{\rm miss} - cp_{\rm miss}$ distributions on the calibration method by changing the binning of the calibration functions. The observed variation of the results are found to be covered by the statistical uncertain-

ties of the calibration functions, and no contribution is added to the total systematic uncertainty.

6. Stability of the results

The stability of the results is tested by dividing the data into several independent subsamples: $B^{\pm}$ and B^0, decays to electrons and muons, different run periods of roughly equal sample sizes, and two regions in the $E_{\rm miss} - cp_{\rm miss}$ spectrum, $-0.5 \leq E_{\rm miss} - cp_{\rm miss} < 0$ GeV and $0 \leq E_{\rm miss} - cp_{\rm miss} < 0.5$ GeV, characterized by different resolutions of the reconstructed hadronic system. No significant variations are observed.

D. Results

The measured hadronic-mass moments $\langle m_X^k \rangle$ after radiative correction with $k = 1 \ldots 6$ as functions of the minimum lepton-momentum $p^*_{\ell,\rm min}$ are shown in Fig. 5. All measurements are correlated since they share subsets of selected events. Tables II and III summarize the numerical results. In most cases we find systematic uncertainties that exceed the statistical uncertainty by a factor of 2.5. The correlation matrix for the moments is given in the EPAPS document [43].

V. MOMENTS OF THE COMBINED MASS-AND-ENERGY SPECTRUM

The measurement of moments of the observable n_X^2, a combination of the mass and energy of the inclusive X_c system, as defined in Eq. (1), is theoretically motivated and is expected to allow a more reliable extraction of the higher-order HQE parameters μ_π^2 and ρ_D^3 [20].

We present measurements of the moments $\langle n_X^2 \rangle$, $\langle n_X^4 \rangle$, and $\langle n_X^6 \rangle$ for different minimum lepton momenta between 0.8 GeV/c and 1.9 GeV/c in the B-meson rest frame.

A. Event selection

Because of the structure of the variable n_X^2 as a difference of two measured values, its measured resolution and bias are worse than for the mass moments. Also, the sensitivity to cuts on $E_{\rm miss} - cp_{\rm miss}$ increases. The average resolution of n_X^2 after the kinematic fit for lepton momenta greater than 0.8 GeV/c is measured to be 1.05 GeV^2 with a bias of -0.11 GeV^2. We therefore introduce stronger requirements on the reconstruction quality of the event. We tighten the criteria on the neutrino observables by requiring $E_{\rm miss} - cp_{\rm miss}$ to be between -0.2 and 0.3 GeV. Because of the stronger requirement, the individual variables $E_{\rm miss}$ and $p_{\rm miss}$ have less influence on the resolution of the reconstructed hadronic system. Therefore, the requirements on the missing energy and the missing momentum in the event are relaxed to $E_{\rm miss} > 0$ GeV and $p_{\rm miss} > 0$ GeV/c, respectively, as these requirements do not yield
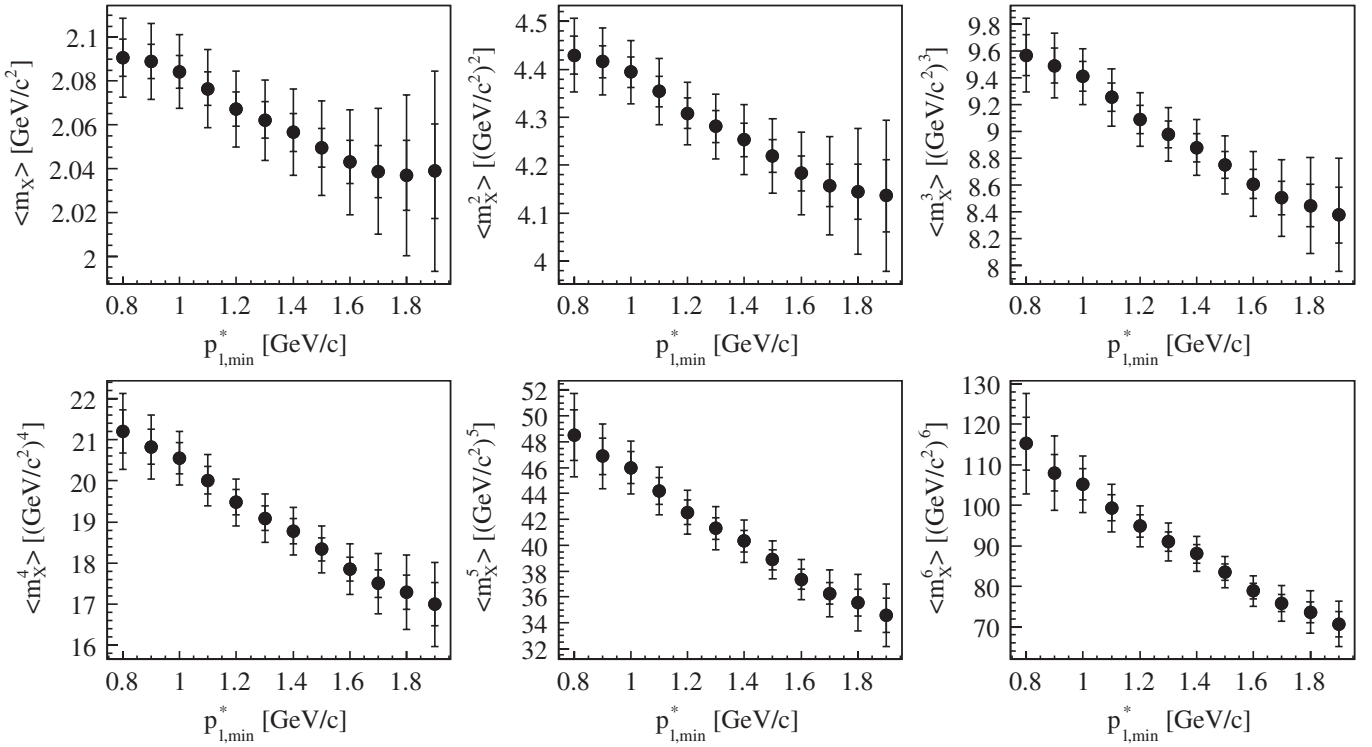
FIG. 5.   Radiation-corrected hadronic-mass moments $\langle m_X^k \rangle$ with $k = 1 \ldots 6$ for different selection criteria on the minimum lepton momentum $p_{\ell,\mathrm{min}}^*$. The inner error bars correspond to the statistical uncertainties while the full error bars correspond to the total uncertainties. The moments, as well as their values for different $p_{\ell,\mathrm{min}}^*$, are highly correlated.

significant improvement on the resolution of n_X^2, and do not increase the ratio of signal to background events.

For $p_\ell^* \geq 0.8$ GeV/c and 1.9 GeV/c, there remain $10,053 \pm 142$ and $1,626 \pm 52$ signal events, respectively. Background events make up 22% of the final event sample with $p_\ell^* \geq 0.8$ GeV/c. The background is composed of 12% continuum and combinatorial background and 10% decays of the signal B meson other than the semileptonic decay $\bar{B} \rightarrow X_c \ell^- \bar{\nu}$. Combinatorial and continuum background is removed using the sideband of the m_{ES} distribution, as described in Sec. III C. The residual background events, containing a correctly reconstructed B_{tag} meson, are removed using MC simulations. The dominant sources are pions misidentified as muons, $\bar{B} \rightarrow X_u \ell^- \bar{\nu}$ decays, and secondary semileptonic decays of D and D_s mesons.

The measured n_X^2 spectra for $p_{\ell,\mathrm{min}}^* = 0.8$ GeV/c and $p_{\ell,\mathrm{min}}^* = 1.9$ GeV/c are shown together with the background distributions in Fig. 6.

B. Extraction of moments

The extraction of unbiased moments $\langle n_X^k \rangle$ from the measured n_X^2 spectra follows a calibration procedure similar to the one used to extract the hadronic-mass moments as described in Sec. IV B. The linear calibration functions

$$n_{X,\mathrm{calib}}^k = \frac{n_{X,\mathrm{reco}}^k - A(E_{\mathrm{miss}} - cp_{\mathrm{miss}}, N_{X_c}, k, p_\ell^*)}{B(E_{\mathrm{miss}} - cp_{\mathrm{miss}}, N_{X_c}, k, p_\ell^*)} \quad (5)$$
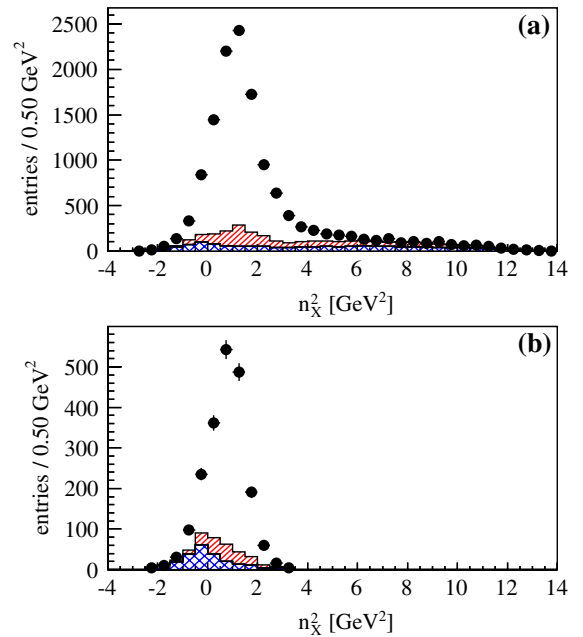

FIG. 6 (color online).   Spectra of n_X^2 after the kinematic fit together with distributions of combinatorial background and background from non-$B\bar{B}$ decays (red, hatched area) as well as residual background (blue, crossed area) for different minimum lepton momenta (a) $p_{\ell,\mathrm{min}}^* = 0.8$ GeV/c and (b) $p_{\ell,\mathrm{min}}^* = 1.9$ GeV/c. The two background histograms are plotted on top of each other.
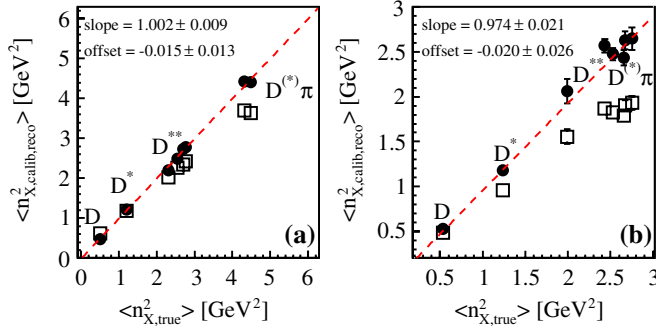
FIG. 7 (color online). Example of the calibration verification procedure for different minimum lepton momenta (a) $p^*_{\ell,\min} = 0.8$ GeV/c and (b) $p^*_{\ell,\min} = 1.7$ GeV/c. Moments $\langle n^2_X \rangle$ of exclusive modes on simulated events before ($\square$) and after ($\bullet$) calibration are plotted against the true moments for each mode. The dotted line shows the result of a fit to the calibrated moments, the resulting parameters are given.

for $k = 2, 4, 6$ are derived from MC samples in three bins of $E_{\mathrm{miss}} - cp_{\mathrm{miss}}$ and three bins of the X_c-system multiplicity N_{X_c} for each of the 12 lepton momentum bins of 100 MeV/c width. Because of differences in events containing electrons and muons, we also derive separate calibration functions for these two classes of events. Overall, we determine 216 linear calibration functions. The calibration again includes the effects of FSR photons which not only modify m_X and p^*_ℓ, but also E_X.

We have verified that applying the calibration procedure on MC samples of individual exclusive $\bar{B} \to X_c \ell^- \bar{\nu}$ modes allows to reproduce the generated moments, as shown in Fig. 7. Small biases remaining after calibration are of the order of 1% for $\langle n^2_X \rangle$ and of few percent for $\langle n^4_X \rangle$ and $\langle n^6_X \rangle$.

Background contributions are removed by applying n^2_X-dependent weight factors $w_i(n^2_X)$ on an event-by-event basis, leading to the following expression for the determination of the moments:

$$\langle n^k_X \rangle = \frac{\sum_{i=1}^{N_{\mathrm{ev}}} w_i(n^2_X) n^k_{X\mathrm{calib},i}}{\sum_{i=1}^{N_{\mathrm{ev}}} w_i(n^2_X)} \times \mathcal{C}(p^*_\ell, k). \qquad (6)$$

The bias correction factors $\mathcal{C}(p^*_\ell, k)$, depending on the minimum lepton momentum and the order of the extracted moments, are determined by MC simulations; they combine the two factors $\mathcal{C}_{\mathrm{cal}}$ and $\mathcal{C}_{\mathrm{true}}$ as described in Sec. IV B.

C. Systematic uncertainties and tests

We consider the same five sources of systematic uncertainties as for the mass moments described in Secs. IV C 1 to IV C 5: MC statistics, simulation-related effects, extraction method, background determination, and modeling of signal decays. The individual contributions to the systematic error, listed in Table IV, are estimated following procedures essentially identical to those described for the mass moments.

Because of the tighter cut on $E_{\mathrm{miss}} - cp_{\mathrm{miss}}$, the systematic uncertainty associated with this criterion is estimated in a different way. We first keep the lower limit fixed to the nominal value and vary the upper limit to 0.3 GeV/c to 0.25 GeV/c, 0.4 GeV/c, and 0.5 GeV/c. Then we fix the upper limit to its nominal value and vary the lower limit to -0.3 GeV/c and -0.1 GeV/c. The mean of the observed differences in the measured moments on data is taken as systematic uncertainty.

In the third study, we include the uncertainty from the binning of the calibration function in the multiplicity of the X_c-system. For the choice of the calibration function, we randomly increase the measured multiplicity of the X_c system by one with a probability of 5% corresponding to the observed difference between MC and data. The uncertainty in the bias-correction factor $\mathcal{C}(p^*_\ell, k)$ is conservatively estimated as half of the applied correction.

Varying the branching fractions of the exclusive signal modes in the MC simulation has, in agreement with the mass-moment studies, a very small impact on the measured combined moments. Also, no significant variations of the results are observed when splitting the data sample into the same subsamples as for the mass moments.

D. Results

Figure 8 shows the results for the moments $\langle n^2_X \rangle$, $\langle n^4_X \rangle$, and $\langle n^6_X \rangle$ as a function of the minimum lepton momentum $p^*_{\ell,\min}$. The moments are highly correlated due to the overlapping data samples. The full numerical results and the statistical and the estimated systematic uncertainties are given in Table IV. The systematic covariance matrix for the moments of different order and with different cuts on $p^*_{\ell,\min}$ is built using statistical correlations. This correlation matrix for the moments is given in the EPAPS document [43].

A clear dependence on the minimum lepton momentum is observed for all moments, due to the increasing contributions from higher-mass final states with decreasing lepton momentum. In most cases we obtain systematic uncertainties slightly exceeding the statistical uncertainty.

VI. MOMENTS OF THE ELECTRON-ENERGY SPECTRUM

Moments of the electron-energy spectrum for semileptonic decays $\bar{B} \to X_c e^- \bar{\nu}$ averaged over charged and neutral B mesons have been measured in a data sample of 51×10^6 $\Upsilon(4S) \to B\bar{B}$ decays [9]. In the following, we present an overview of this analysis and update the results by using more recent measurements [21,41] of branching fractions of background processes.

In multihadron events as defined in [9], $B\bar{B}$ events are selected by requiring a semileptonic B decay with an identified electron (e_{tag}), with charge $Q(e_{\mathrm{tag}})$ and a momentum $1.4 < p^*_e < 2.3$ GeV/c, measured in the $\Upsilon(4S)$ rest frame. These events constitute a tagging sample used as normalization for the branching fraction. A second

TABLE IV.   Results for $\langle n_X^k \rangle$ for $k = 2, 4, 6$ for all minimum lepton-momentum values $p_{\ell,\min}^*$. The statistical uncertainty contains the uncertainty arising from the limited data sample and an additional statistical uncertainty arising from the determination of the combinatorial background. The systematic uncertainties are grouped in five categories having related sources: *MC statistics* contains the statistical uncertainties of the calibration curves and of the residual background. *Simulation related* is the sum of neutral and charged reconstruction efficiency differences in data and MC, $E_{\mathrm{miss}} - cp_{\mathrm{miss}}$ differences, mismodeling of final state radiation, and PID impact. The category *extraction method* contains the conservative estimate of half of the bias correction and the impact of the calibration curve binning. The category *background* sums all contributions from the variation of the residual background components. The category *signal model* sums the impact of the variation of the signal decay branching fractions.

k	$p_{\ell,\min}^*$ [GeV/c]	$\langle n_X^k \rangle$		σ_{stat}		σ_{sys}	MC statistics	simulation related	extraction method	background	signal model
2	0.8	1.522	±	0.049	±	0.056	0.020	0.050	0.011	0.012	0.004
	0.9	1.483	±	0.047	±	0.057	0.015	0.054	0.009	0.009	0.004
	1.0	1.465	±	0.044	±	0.041	0.013	0.037	0.009	0.008	0.003
	1.1	1.438	±	0.037	±	0.040	0.012	0.037	0.009	0.006	0.003
	1.2	1.449	±	0.034	±	0.038	0.011	0.036	0.006	0.005	0.002
	1.3	1.428	±	0.031	±	0.031	0.010	0.027	0.006	0.006	0.004
	1.4	1.400	±	0.030	±	0.028	0.009	0.025	0.006	0.006	0.004
	1.5	1.369	±	0.035	±	0.032	0.009	0.029	0.008	0.007	0.005
	1.6	1.346	±	0.033	±	0.027	0.009	0.020	0.014	0.007	0.003
	1.7	1.344	±	0.037	±	0.029	0.010	0.020	0.015	0.008	0.004
	1.8	1.337	±	0.038	±	0.035	0.013	0.014	0.029	0.008	0.004
	1.9	1.196	±	0.032	±	0.033	0.017	0.017	0.020	0.009	0.003
4	0.8	3.54	±	0.41	±	0.39	0.14	0.34	0.08	0.10	0.03
	0.9	3.21	±	0.37	±	0.36	0.11	0.32	0.09	0.05	0.02
	1.0	3.00	±	0.29	±	0.25	0.09	0.21	0.09	0.04	0.02
	1.1	2.74	±	0.22	±	0.17	0.06	0.14	0.09	0.01	0.02
	1.2	2.81	±	0.19	±	0.20	0.06	0.15	0.12	0.02	0.03
	1.3	2.60	±	0.15	±	0.16	0.04	0.10	0.11	0.01	0.04
	1.4	2.51	±	0.13	±	0.12	0.04	0.08	0.09	0.01	0.03
	1.5	2.34	±	0.13	±	0.13	0.03	0.09	0.09	0.00	0.02
	1.6	2.11	±	0.10	±	0.09	0.03	0.06	0.06	0.00	0.01
	1.7	2.03	±	0.12	±	0.08	0.03	0.06	0.04	0.00	0.01
	1.8	1.98	±	0.10	±	0.06	0.04	0.04	0.02	0.00	0.01
	1.9	1.57	±	0.07	±	0.06	0.03	0.05	0.02	0.00	0.01
6	0.8	13.52	±	3.93	±	3.42	1.37	2.97	0.49	0.81	0.34
	0.9	10.87	±	2.78	±	2.65	0.93	2.39	0.52	0.37	0.24
	1.0	9.02	±	2.22	±	1.88	0.84	1.55	0.54	0.29	0.20
	1.1	7.06	±	1.35	±	0.78	0.35	0.58	0.34	0.07	0.14
	1.2	7.50	±	1.16	±	0.92	0.32	0.68	0.49	0.11	0.18
	1.3	6.28	±	0.84	±	0.64	0.22	0.38	0.41	0.06	0.20
	1.4	5.83	±	0.62	±	0.49	0.16	0.30	0.32	0.06	0.12
	1.5	4.99	±	0.49	±	0.52	0.13	0.30	0.40	0.03	0.05
	1.6	3.93	±	0.32	±	0.31	0.11	0.16	0.24	0.03	0.03
	1.7	3.63	±	0.35	±	0.22	0.09	0.13	0.15	0.02	0.03
	1.8	3.42	±	0.23	±	0.19	0.09	0.11	0.12	0.02	0.03
	1.9	2.51	±	0.16	±	0.13	0.06	0.11	0.03	0.02	0.02

electron e_{sig}, for which we require $p_e^* > 0.5$ GeV/c, is assigned either to the unlike-sign sample if the tagged sample contains an electron with $Q(e_{\mathrm{tag}}) = -Q(e_{\mathrm{sig}})$ or to the like-sign sample if $Q(e_{\mathrm{tag}}) = Q(e_{\mathrm{sig}})$. In events without $B^0 \bar{B}^0$ mixing, primary electrons from semileptonic B decays belong to the unlike-sign sample while secondary electrons contribute to the like-sign sample. Secondary electrons originating from the same B as the e_{tag} are removed from the unlike-sign sample by the requirement

$$\cos\alpha^* > 1.0 - p_e^* \ c/\mathrm{GeV} \quad \text{and} \quad \cos\alpha^* > -0.2, \quad (7)$$

where α^* is the angle between the two electrons in the $\Upsilon(4S)$ rest frame. Corrections for the small residual background of unlike-sign pairs originating from the same B fulfilling this requirement are described in [9]. Additional background corrections for electrons from $J/\psi \to e^+ e^-$ decays, continuum events, photon conversions, $\pi^0 \to e^+ e^- \gamma$ Dalitz decays, and misidentified hadrons are also
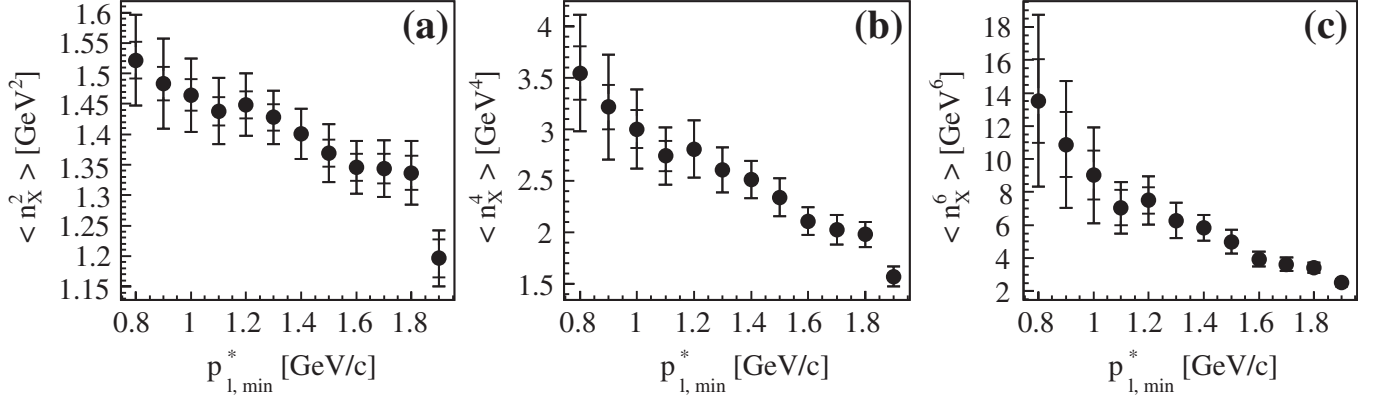
FIG. 8. Radiation-corrected moments (a) $\langle n_X^2 \rangle$, (b) $\langle n_X^4 \rangle$, and (c) $\langle n_X^6 \rangle$ for different cuts on the lepton momentum p_ℓ^*. The inner error bars correspond to the statistical uncertainties while the full error bars correspond to the total uncertainties. The moments are highly correlated.
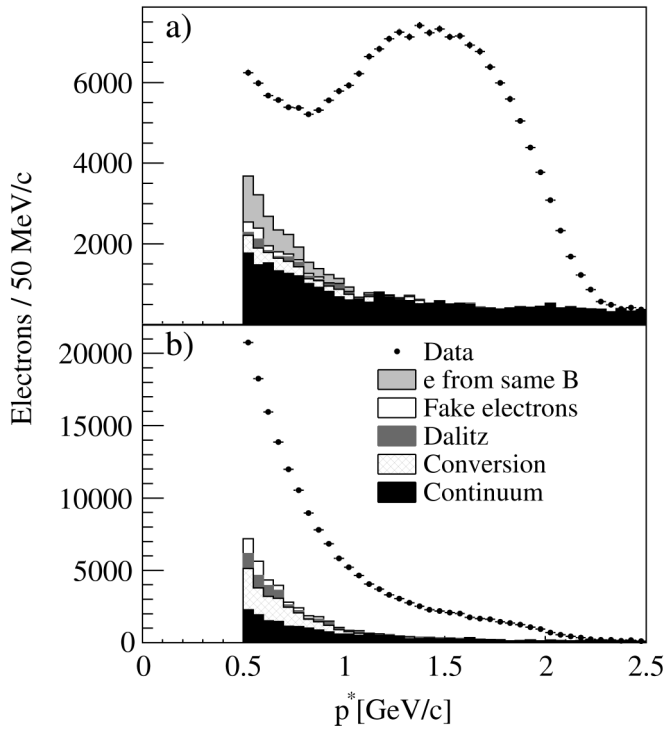

FIG. 9. Previously measured momentum spectrum (points) [9] and estimated backgrounds (histograms) for electron candidates in (a) the unlike-sign sample, and (b) the like-sign sample. The background spectra are updated w.r.t. the previous publication with more recent branching-fraction measurements [21,41].

described in [9]. Figure 9 shows the electron-momentum spectra together with the contributions of the backgrounds.

Further backgrounds arise from decays of τ leptons, charmed mesons produced in $b \rightarrow c\bar{c}s$ decays, and J/ψ or $\psi(2S) \rightarrow e^+e^-$ decays with only one detected electron. We also need to correct for cases where the tagged electron does not originate from a semileptonic B decay. These backgrounds are irreducible. Their contributions to the three samples—single electrons, like-sign, and unlike-sign pairs—are estimated from MC simulations, using the ISGW2 model [36] to describe semileptonic D and D_s-meson decays. As an important update to the results in [9], the branching fractions of these backgrounds are re-calculated to match the recent measurements [21]. As in [9], we calculate $\mathcal{B}(D_s \rightarrow Xe\nu) = (7.79 \pm 0.19)\%$ from $\mathcal{B}(D^0 \rightarrow Xe\nu)$ and $\mathcal{B}(D^+ \rightarrow Xe\nu)$, assuming $\Gamma(D_s \rightarrow Xe\nu) = \Gamma(D \rightarrow Xe\nu)$. Using $\mathcal{B}(B^{0,+} \rightarrow D_s^+X) = (8.3 \pm 0.8)\%$ [21] the branching fraction of $B^{0,+} \rightarrow D_s^+ \rightarrow e^+$ decays, where the D_s originates from fragmentation of the W boson, is $(0.65 \pm 0.06)\%$. Using the inclusive branching-fraction measurement of $B^{0,+} \rightarrow D^{0,+}X$ decays reported in [41], we arrive at $\mathcal{B}(B^{0,+} \rightarrow D^{0,+} \rightarrow e^+) = (0.93 \pm 0.11)\%$. To estimate the contribution of electrons from τ decays, we consider the cascades $B \rightarrow \tau \rightarrow e$ and $B \rightarrow D_s \rightarrow \tau \rightarrow e$, with branching fractions taken from [21]. The rates for the decays $B \rightarrow J/\psi \rightarrow e^+e^-$ and $B \rightarrow \psi(2S) \rightarrow e^+e^-$ are also adjusted to [21].

After the like- and unlike-sign samples have been corrected for electron identification efficiency, these irreducible background spectra are subtracted. To account for $B^0\bar{B}^0$ mixing, we determine the number of primary electrons in the i-th p^*-bin from the like-sign and unlike-sign pairs as

$$N_{b \rightarrow c,u}^i = \frac{N_{e^+e^-}^i}{\epsilon_{\alpha^*}^i} \frac{(1 - f_0\chi_0) - (1 - \rho)(1 - f_0)}{(1 - 2f_0\chi_0) - (1 - \rho)(1 - f_0)(1 - f_0\chi_0)} + N_{e^\pm e^\pm}^i \frac{f_0\chi_0}{(1 - 2f_0\chi_0) - (1 - \rho)(1 - f_0)(1 - f_0\chi_0)} \quad (8)$$
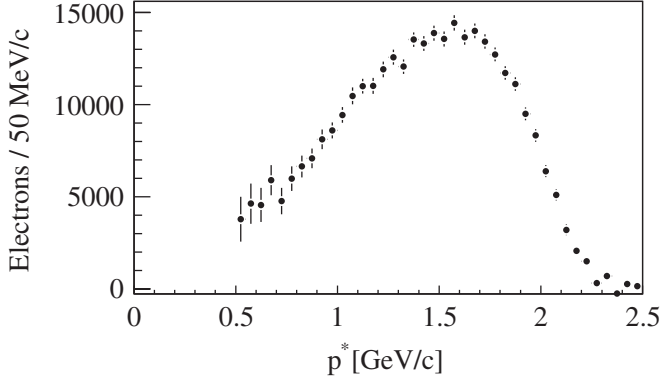
FIG. 10. Electron-momentum spectrum from $B \to X e \nu (\gamma)$ decays in the $\Upsilon(4S)$ frame after correction for efficiencies and bremsstrahlung in the detector, with combined statistical and systematic errors.

where $\chi_0 = 0.1878 \pm 0.0024$ [21] is the $B^0 \bar{B}^0$ mixing parameter, $f_0 = \mathcal{B}(\Upsilon(4S) \to B^0 \bar{B}^0) = 0.491 \pm 0.007$ [21], and $\rho = \mathcal{B}(B^+ \to \bar{D}^0 \to e^-)/\mathcal{B}(B^0 \to D^- \to e^-) = (0.744 \pm 0.06)$ [21]. The parameter $\epsilon_{\alpha^*}^i$ is the efficiency of the additional requirement for the unlike-sign sample as defined in Eq. (7). The spectrum obtained from Eq. (8) is corrected for the effects of bremsstrahlung in the detector material using MC simulation. Figure 10 shows the resulting spectrum of primary electrons.

We determine the partial branching fraction as $(\sum_i N_{b \to c,u}^i)/(N_{tag} \epsilon_{evt} \epsilon_{cuts})$, where i runs over all bins with $E_e > E_0$. For the background-corrected number N_{tag} of tag electrons we find $N_{tag} = (3617 \pm 4 \pm 22) \times 10^3$, where the uncertainties are statistical and systematic, respectively. The parameter $\epsilon_{evt} = (98.9 \pm 0.5)\%$ refers to the relative efficiency for selecting two-electron events compared to events with a single e_{tag}, and $\epsilon_{cuts} = (82.8 \pm 0.3)\%$ is the acceptance for the signal electron for $E_0 = 0.6$ GeV. The result is

$$\mathcal{B}(B \to X e \nu (\gamma), E_e > 0.6 \text{ GeV}) = (10.30 \pm 0.06 \pm 0.21)\%,$$

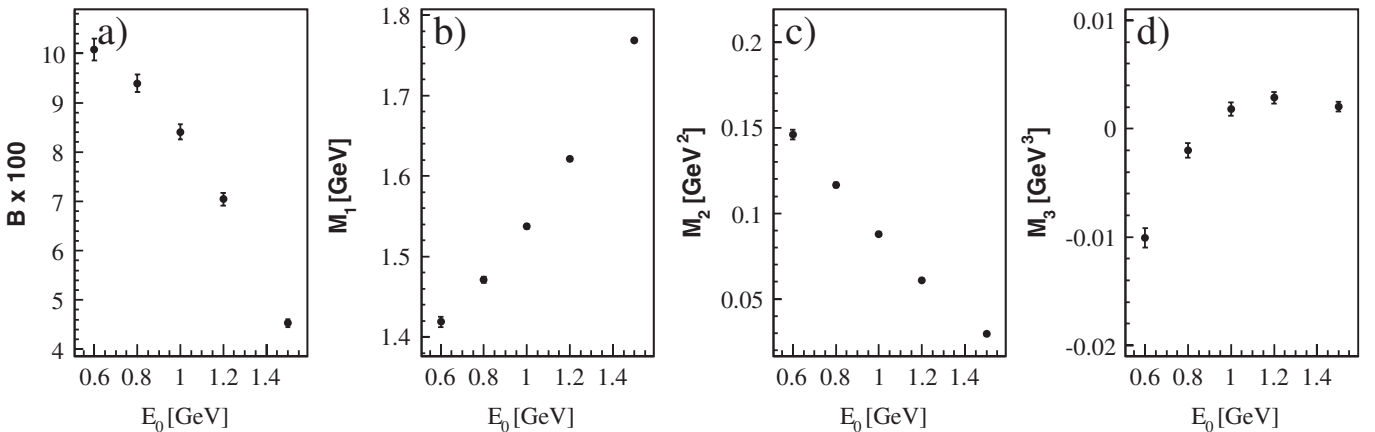where the errors correspond to the statistical and systematic uncertainties, respectively.

In the B-meson rest frame, we define $R_i(E_0, \mu)$ as $\int_{E_0}^{\infty} (E_e - \mu)^i (d\Gamma/dE_e) dE_e$, and measure the first moment $M_1(E_0) = R_1(E_0, 0)/R_0(E_0, 0)$, the central moments $M_n(E_0) = R_n(E_0, M_1(E_0))/R_0(E_0, 0)$ for $n = 2, 3$ and the partial branching-fraction $\mathcal{B}(E_0) = \tau_B R_0(E_0, 0)$, where τ_B is the average lifetime of charged and neutral B mesons. The calculation of the moments is done as in [9] and includes corrections for charmless semileptonic decays, the movement of the B mesons in the c.m. frame, biases due to the event selection criteria, and binning effects. The spectra and moments presented are those of $B \to X_c e \nu (\gamma)$ decays with any number of photons. Since current theoretical predictions on the lepton-energy moments do not incorporate photon emission, we also present a second set of moments with corrections for the impact of QED radiation using the PHOTOS code [26].

Figure 11 shows the moments of $B \to X_c e \nu (\gamma)$ decays as a function of E_0, and Table V lists the main systematic errors for $E_0 = 0.6$ and 1.5 GeV. The complete listing of all moments and the full correlation matrix, with and without PHOTOS corrections can be found in [43].

VII. DETERMINATION OF $|V_{cb}|$ AND THE QUARK MASSES m_b AND m_c

At the parton level, the weak decay rate for $b \to c \ell \nu$ can be calculated accurately; it is proportional to $|V_{cb}|^2$ and depends on the quark masses m_b and m_c. To relate measurements of the semileptonic B-meson decay rate to $|V_{cb}|$, the parton-level calculations have to be corrected for effects of strong interactions. Heavy Quark Expansions (HQEs) [44–46] have become a successful tool for calculating perturbative and nonperturbative QCD corrections [47–51] and for estimating their uncertainties.

In the kinetic-mass scheme [11,20,52–55], these expansions in $1/m_b$ and the strong coupling constant $\alpha_s(m_b)$ to

FIG. 11. Measured branching fraction (a) and moments M_1 (b), M_2 (c), and M_3 (d) of the inclusive electron-energy spectrum of $B \to X_c e \nu (\gamma)$ decays as a function of the cutoff energy E_0 in the B-meson rest frame.

TABLE V. Results and breakdown of the systematic errors for the partial branching fraction $\mathcal{B} = \tau_B \int_{E_0}^{\infty} (d\Gamma/dE_e) dE_e$, and the moments M_1, M_2, and M_3 for $B \to X_c e\nu$ and $B \to X_c e\nu(\gamma)$ in the B-meson rest frame for two values of E_0. Changes w.r.t. the previously published results [9] are due to updated background branching fractions [21,41] and indicated by (†).

	$\mathcal{B}[10^{-2}]$		M_1 [MeV]		$M_2[10^{-3}$ GeV$^2]$		$M_3[10^{-3}$ GeV$^3]$	
E_0 [GeV]	0.6	1.5	0.6	1.5	0.6	1.5	0.6	1.5
				Breakdown of systematic errors				
Conversion and Dalitz pairs	0.028	0.001	1.5	0.02	0.6	0.00	0.04	0.00
e identification efficiency	0.150	0.044	2.5	0.30	0.6	0.07	0.27	0.08
e from same B	0.019	0.000	1.3	0.00	0.6	0.00	0.05	0.00
$B \to D_s \to e$ (†)	0.024	0.000	1.4	0.01	0.5	0.00	0.03	0.00
$B \to D \to e$ (†)	0.035	0.000	2.2	0.00	1.0	0.00	0.03	0.00
$B \to \tau \to e$ (†)	0.027	0.001	1.2	0.04	0.3	0.00	0.10	0.00
e from J/ψ or $\psi(2S)$ (†)	0.002	0.001	0.0	0.01	0.0	0.01	0.00	0.00
Secondary tags	0.052	0.011	1.6	0.06	0.6	0.00	0.05	0.00
χ	0.022	0.011	0.9	0.01	0.3	0.00	0.03	0.00
Tracking efficiency	0.083	0.033	1.0	0.06	0.3	0.02	0.06	0.00
Bremsstrahlung correction	0.011	0.028	1.9	0.43	0.0	0.05	0.18	0.00
Event selection	0.052	0.024	0.6	0.14	0.0	0.03	0.07	0.01
$b \to u$ subtraction (†)	0.031	0.020	0.8	0.83	0.4	0.32	0.14	0.12
B momentum correction	0.000	0.005	0.0	0.19	0.1	0.10	0.04	0.02
N_{tag} normalization	0.068	0.030						
				Results				
Results for $B \to X_c e\nu(\gamma)$	10.08	4.53	1418.8	1768.7	146.1	29.6	-10.08	2.04
$\pm$(stat.)	0.06	0.03	3.8	1.9	2.0	0.8	0.81	0.44
$\pm$(syst.)	0.21	0.08	5.4	1.0	1.9	0.4	0.40	0.15
Results for $B \to X_c e\nu$	10.20	4.78	1437.6	1773.7	145.4	30.1	-12.04	2.04
$\pm$(stat.)	0.06	0.03	4.0	1.9	2.3	0.9	0.91	0.47
$\pm$(syst.)	0.22	0.08	5.7	1.1	2.1	0.4	0.40	0.15

order $\mathcal{O}(1/m_b^3)$ contain six parameters: the running kinetic masses of the b and c quarks, $m_b(\mu)$ and $m_c(\mu)$, and four nonperturbative parameters. The parameter μ denotes the Wilson factorization scale that separates effects from long- and short-distance dynamics. The calculations are performed for $\mu = 1$ GeV [56]. It has been shown that the expressions for the moments have only a small scale dependence [17]. We determine these six parameters and $|V_{cb}|$ from fits to moments of the hadronic-mass, combined mass-and-energy, and electron-energy distributions in semileptonic B decays $\bar{B} \to X_c \ell^- \bar{\nu}$ and moments of the photon-energy spectrum in decays $\bar{B} \to X_s \gamma$ [14–16].

In the kinetic-mass scheme the HQE to $\mathcal{O}(1/m_b^3)$ for the rate Γ_{SL} of semileptonic decays $\bar{B} \to X_c \ell^- \bar{\nu}$ can be expressed as [11]

$$\Gamma_{SL} = \frac{G_F^2 m_b^5}{192\pi^3} |V_{cb}|^2 (1 + A_{\text{ew}}) A_{\text{pert}}(r, \mu) \left[z_0(r) \left(1 - \frac{\mu_\pi^2 - \mu_G^2 + \frac{\rho_D^3 + \rho_{LS}^3}{c^2 m_b}}{2c^4 m_b^2} \right) - 2(1 - r)^4 \frac{\mu_G^2 + \frac{\rho_D^3 + \rho_{LS}^3}{c^2 m_b}}{c^4 m_b^2} + d(r) \frac{\rho_D^3}{c^6 m_b^3} + \mathcal{O}(1/m_b^4) \right].$$

(9)

The leading nonperturbative effects arise at $\mathcal{O}(1/m_b^2)$ and are parametrized by $\mu_\pi^2(\mu)$ and $\mu_G^2(\mu)$, the expectation values of the kinetic and chromomagnetic dimension-five operators. At $\mathcal{O}(1/m_b^3)$, two additional parameters enter, $\rho_D^3(\mu)$ and $\rho_{LS}^3(\mu)$, the expectation values of the Darwin and spin-orbit dimension-six operators, respectively. The ratio $r = m_c^2/m_b^2$ enters in the tree level phase space factor $z_0(r) = 1 - 8r + 8r^3 - r^4 - 12r^2 \ln r$ and in the function $d(r) = 8 \ln r + 34/3 - 32r/3 - 8r^2 + 32r^3/3 - 10r^4/3$. The factor $1 + A_{\text{ew}}$ accounts for elec-troweak corrections. It is estimated to be $1 + A_{\text{ew}} \cong (1 + \alpha/\pi \ln M_Z/m_b)^2 = 1.014$, where α is the electromagnetic coupling constant. The quantity A_{pert} accounts for perturbative contributions and is estimated to be $A_{\text{pert}}(r, \mu) \approx 0.908$ [11].

The performed fit uses a linearized expression for the dependence of $|V_{cb}|$ on the values of heavy-quark parameters, expanded around *a priori* estimates of these parameters [11]:

$$\frac{|V_{cb}|}{0.0417} = \sqrt{\frac{\mathcal{B}(\bar{B} \to X_c \ell^- \bar{\nu})}{0.1032} \frac{1.55}{\tau_B}}[1 + 0.30(\alpha_s(m_b) - 0.22)][1 - 0.66(m_b - 4.60) + 0.39(m_c - 1.15)$$

$$+ 0.013(\mu_\pi^2 - 0.40) + 0.09(\rho_D^3 - 0.20) + 0.05(\mu_G^2 - 0.35) - 0.01(\rho_{LS}^3 + 0.15)]. \tag{10}$$

Here m_b and m_c are in GeV/c^2 and all other parameters of the expansion are in GeV^k; τ_B refers to the average lifetime of B mesons produced at the $\Upsilon(4S)$, measured in picoseconds. HQEs in terms of the same heavy-quark parameters are available for hadronic-mass, combined mass-and-energy, electron-energy, and photon-energy moments. Predictions for those moments are obtained from an analytical calculation [57]. We use these calculations to determine $|V_{cb}|$, the total semileptonic branching fraction $\mathcal{B}(\bar{B} \to X_c \ell^- \bar{\nu})$, the quark masses m_b and m_c, as well as the heavy-quark parameters μ_π^2, μ_G^2, ρ_D^3, and ρ_{LS}^3, from a simultaneous χ^2 fit to the measured moments and partial branching fractions, all as functions of the minimum lepton momentum $p_{\ell,\text{min}}^*$ and minimum photon energy $E_{\gamma,\text{min}}$.

A. Extraction formalism

The fit method designed to extract the HQE parameters from the measured moments has been reported previously [17,58]. It is based on a χ^2 minimization,

$$\chi^2 = (\vec{M}_{\text{exp}} - \vec{M}_{\text{HQE}})^T \mathcal{C}_{\text{tot}}^{-1} (\vec{M}_{\text{exp}} - \vec{M}_{\text{HQE}}). \tag{11}$$

The vectors $\vec{M}_{\text{exp}}$ and $\vec{M}_{\text{HQE}}$ contain the measured moments and the corresponding moments calculated by theory, respectively. Furthermore, the expression in Eq. (11) contains the total covariance matrix $\mathcal{C}_{\text{tot}} = \mathcal{C}_{\text{exp}} + \mathcal{C}_{\text{HQE}}$ defined as the sum of the experimental $\mathcal{C}_{\text{exp}}$ and theoretical $\mathcal{C}_{\text{HQE}}$ covariance matrices (see Sec. VII C).

The total semileptonic branching fraction $\mathcal{B}(\bar{B} \to X_c \ell^- \bar{\nu})$ is extracted in the fit by extrapolating the measured partial branching fractions $\mathcal{B}_{p_{\ell,\text{min}}^*}(\bar{B} \to X_c \ell^- \bar{\nu})$ with $p_\ell^* \geq p_{\ell,\text{min}}^*$ to the full lepton-energy spectrum. Using HQE predictions of the relative decay fraction

$$R_{p_{\ell,\text{min}}^*} = \frac{\int_{p_{\ell,\text{min}}^*} \frac{d\Gamma_{SL}}{dp_\ell^*} dp_\ell^*}{\int_0 \frac{d\Gamma_{SL}}{dp_\ell^*} dp_\ell^*}, \tag{12}$$

the total branching fraction can be introduced as a free parameter in the fit. It is given by

$$\mathcal{B}(\bar{B} \to X_c \ell^- \bar{\nu}) = \frac{\mathcal{B}_{p_{\ell,\text{min}}^*}(\bar{B} \to X_c \ell^- \bar{\nu})}{R_{p_{\ell,\text{min}}^*}}. \tag{13}$$

Using Eqs. (10) and (11) together with the measured average B-meson lifetime τ_B and the total branching fraction, allows the calculation of $|V_{cb}|$:

$$|V_{cb}|^2 \propto \Gamma_{SL} = \frac{\mathcal{B}(\bar{B} \to X_c \ell^- \bar{\nu})}{\tau_B}. \tag{14}$$

Thereby, $|V_{cb}|$ is introduced as an additional free parameter to the fit. To propagate the uncertainty on τ_B properly into the extracted result for $|V_{cb}|$, τ_B is added as an additional measurement to the vectors of measured and predicted quantities, $\vec{M}_{\text{exp}}$ and $\vec{M}_{\text{HQE}}$.

The nonperturbative parameters μ_G^2 and ρ_{LS}^3 have been estimated from the B-B^* mass splitting and heavy-quark sum rules to be $\mu_G^2 = (0.35 \pm 0.07)$ GeV^2 and $\rho_{LS}^3 = (-0.15 \pm 0.10)$ GeV^3 [17], respectively. Both parameters are restricted in the fit by imposing Gaussian error constraints.

B. Experimental input

The combined fit is performed on a subset of available moment measurements with correlations below 95% to ensure the invertability of the covariance matrix. Since the omitted measurements are characterized by high correlations to other measurements considered in the fit, they do not contribute significant additional information, and the overall sensitivity of the results is not affected. Choosing a different subset of moments gives consistent results. We perform two fits to the following set of measured moments, thereby including either the hadronic-mass moments or the moments of the combined mass-and-energy spectrum:

(i) Hadronic-mass moments are used as presented in this paper. We select the following subset for the fit: $\langle m_X^2 \rangle$ for $p_\ell^* \geq 0.9, 1.1, 1.3, 1.5$ GeV/c, $\langle m_X^4 \rangle$ for $p_\ell^* \geq 0.8, 1.0, 1.2, 1.4$ GeV/c, and $\langle m_X^6 \rangle$ for $p_\ell^* \geq 0.9, 1.1, 1.3, 1.5$ GeV/c.

(ii) Moments of the combined mass-and-energy spectrum as presented in this paper. The following subset of moments is included in the fit: $\langle n_X^2 \rangle$ for $p_\ell^* \geq 0.9, 1.1, 1.3, 1.5$ GeV/c, $\langle n_X^4 \rangle$ for $p_\ell^* \geq 0.8, 1.0, 1.2, 1.4$ GeV/c, and $\langle n_X^6 \rangle$ for $p_\ell^* \geq 0.9, 1.1, 1.3, 1.5$ GeV/c.

Both fits include the updated lepton-energy moments as presented in this paper with radiative corrections as well as photon-energy moments measured in $\bar{B} \to X_s \gamma$ decays as presented in [14–16]. We use the partial branching fraction $\mathcal{B}_{p_{\ell,\text{min}}^*}$ measured for $p_\ell^* \geq 0.6, 1.0, 1.5$ GeV/c and the moments $\langle E_\ell \rangle$ for $p_\ell^* \geq 0.6, 0.8, 1.0, 1.2, 1.5$ GeV/c. The lepton-energy moments $\langle E_\ell^2 \rangle$ are used for the minimum lepton momentum $p_\ell^* \geq 0.6, 1.0, 1.5$ GeV/c and $\langle E_\ell^3 \rangle$ for $p_\ell^* \geq 0.8, 1.2$ GeV/c. We include the photon-energy moments $\langle E_\gamma \rangle$ for the minimum photon energies
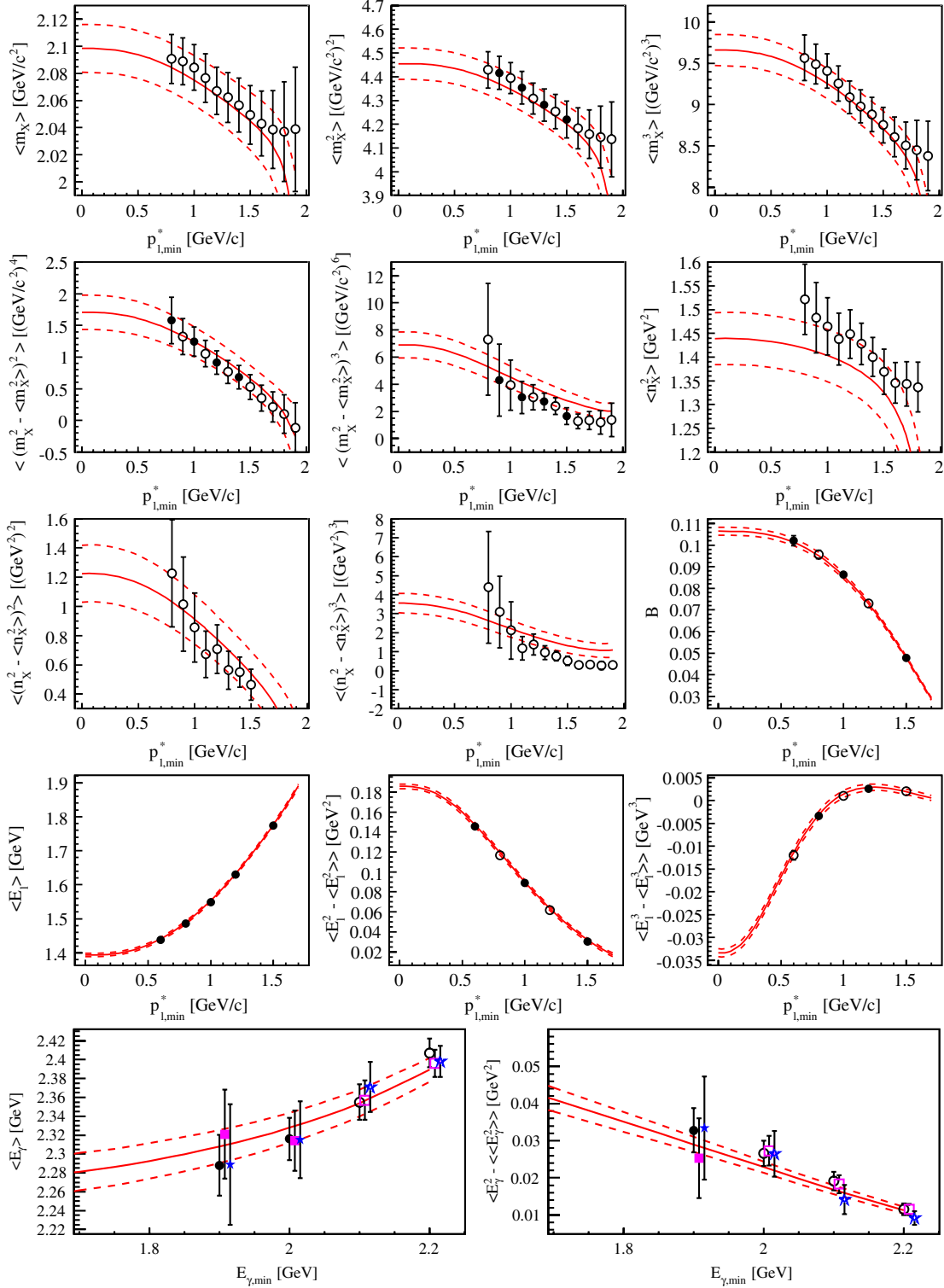
FIG. 12 (color online). The measured hadronic-mass moments $\langle m_X^k \rangle$, combined mass-and-energy moments $\langle n_X^k \rangle$, electron-energy moments $\langle E_\ell^k \rangle$, partial branching fractions B, and photon-energy moments $\langle E_\gamma^n \rangle$, as a function of the minimum lepton momentum $p_{\ell,\min}^*$ and minimum photon energy $E_{\gamma,\min}$ compared with the result of the simultaneous fit (solid line) to moments of the hadronic mass spectrum, electron-energy moments, and photon-energy moments. The solid data points mark the measurements included in the fit. Moments of semileptonic decays $\bar{B} \rightarrow X_c \ell^- \bar{\nu}$ are marked by ($\bullet$). Photon-energy moments of Ref. [14] are marked by ($\blacksquare$), of Ref. [15] by ($\bullet$), and of Ref. [16] by ($\star$). Open data points are not used in the fit. The vertical bars indicate the experimental errors. The dashed lines correspond to the total fit uncertainty as obtained by converting the fit errors of each individual HQE parameter into an error for the individual moment.

$E_\gamma \geq 1.9$ GeV and $E_\gamma \geq 2.0$ GeV, and $\langle E_\gamma^2 \rangle$ for $E_\gamma \geq 1.9$ GeV. In addition, we use $\tau_B = f_0 \tau_0 + (1 - f_0)\tau_\pm = (1.585 \pm 0.007)$ ps, taking into account the lifetimes [21] of neutral and charged B mesons, τ_0 and $\tau_\pm$, and their relative production rates, $f_0 = 0.491 \pm 0.007$ [21].

C. Theoretical uncertainties

As discussed in [17] and specified in [20], the following theoretical uncertainties are taken into account:

The uncertainty related to the uncalculated perturbative corrections to the Wilson coefficients of nonperturbative operators are estimated by varying the corresponding parameters μ_π^2 and μ_G^2 by 20% and ρ_D^3 and ρ_{LS}^3 by 30% around their expected values. Uncertainties for the perturbative corrections are estimated by varying α_s up and down by 0.1 for the hadronic-mass moments and by 0.04 for the lepton-energy moments around its nominal value of $\alpha_s = 0.22$. Uncertainties in the perturbative corrections of the quark masses m_b and m_c are addressed by varying both by 20 MeV/c^2 up and down around their expected values.

For the extracted value of $|V_{cb}|$ an additional error of 1.4% is added for the uncertainty in the expansion of the semileptonic rate Γ_{SL} [11,55]. It accounts for remaining uncertainties in the perturbative corrections to the leading operator, uncalculated perturbative corrections to the chromomagnetic and Darwin operator, higher-order power corrections, and possible nonperturbative effects in the operators with charm fields. This uncertainty is not included in the theoretical covariance matrix $\mathcal{C}_{\text{HQE}}$ but is listed separately as a theoretical uncertainty on $|V_{cb}|$.

For the predicted photon-energy moments $\langle E_\gamma^n \rangle$, additional uncertainties are taken into account. As outlined in [52], uncertainties of 30% of the applied bias correction to the photon-energy moments and half the difference in the moments derived from two different distribution-function *ansätze* have to be considered. Both contributions are added linearly [17].

The theoretical covariance matrix $\mathcal{C}_{\text{HQE}}$ is constructed by assuming fully correlated theoretical uncertainties for a given moment with different lepton-momentum or photon-energy cutoffs and assuming uncorrelated theoretical uncertainties for moments of different orders and types. The additional uncertainties considered for the photon-energy moments are assumed to be uncorrelated for different moments and photon-energy cutoffs.

D. Results

In the following, the results of the two fits, one including the measurement of hadronic-mass moments and the other including the measured moments of the combined mass-and-energy spectrum instead, are discussed.

We use a parametrized MC simulation to separate the fit parameter uncertainties into experimental and theoretical contributions. The simulation starts from a single set of moments which is obtained by calculating predictions for all moments from the nominal fit parameter results. We generate 250 sets of pseudo measurements of moments by varying the moments randomly with the covariance matrices $\mathcal{C}_{\text{tot}}$ or $\mathcal{C}_{\text{exp}}$. The means of the squared errors of the parameters i obtained from the fits to the pseudo measurements give the MC squared total errors $\hat{\Delta}_{i,\text{tot}}^2$ and the MC squared experimental errors $\hat{\Delta}_{i,\text{exp}}^2$, respectively. The squared theoretical uncertainties are calculated as $\hat{\Delta}_{i,\text{theo}}^2 = \hat{\Delta}_{i,\text{tot}}^2 - \hat{\Delta}_{i,\text{exp}}^2$. The quoted final uncertainties are obtained by rescaling the experimental and theoretical uncertainties of the MC simulation with factors $\Delta_{i,\text{tot}}/\hat{\Delta}_{i,\text{tot}}$, where $\Delta_{i,\text{tot}}$

TABLE VI. Results of the simultaneous fit to moments of the hadronic-mass spectrum, electron-energy moments, and photon-energy moments. For $|V_{cb}|$ we account for an additional theoretical uncertainty of 1.4% from the uncertainty in the expansion of Γ_{SL}. Correlation coefficients for all parameters are summarized below the central values.

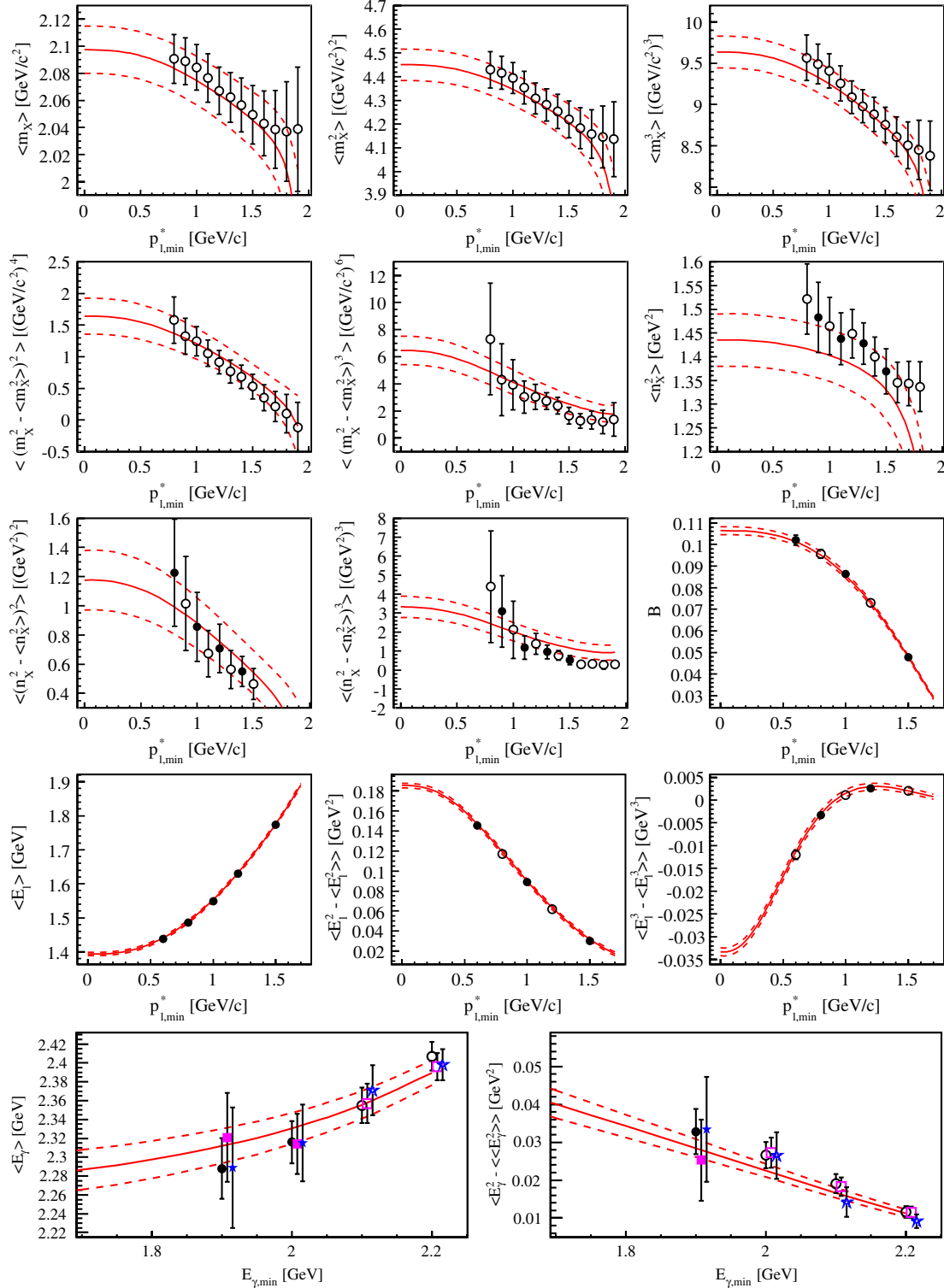|	$|V_{cb}| \times 10^3$	m_b [GeV/c^2]	m_c [GeV/c^2]	$\mathcal{B}$ [%]	μ_π^2 [GeV/c^2]	μ_G^2 [GeV/c^2]	ρ_D^3 [GeV/c^3]	ρ_{LS}^3 [GeV/c^3]
Results	42.05	4.549	1.077	10.642	0.476	0.300	0.203	-0.144
Δ_{exp}	0.45	0.031	0.041	0.165	0.021	0.044	0.017	0.075
Δ_{theo}	0.37	0.038	0.062	0.063	0.059	0.038	0.027	0.056
$\Delta_{\Gamma_{SL}}$	0.59							
Δ_{tot}	0.83	0.049	0.074	0.176	0.063	0.058	0.032	0.094
$|V_{cb}|$	1.00	-0.33	-0.11	0.76	0.32	-0.42	0.40	0.12
m_b		1.00	0.95	0.08	-0.52	0.14	-0.22	-0.24
m_c			1.00	0.15	-0.56	-0.12	-0.21	-0.15
$\mathcal{B}$				1.00	0.16	-0.09	0.16	-0.06
μ_π^2					1.00	0.04	0.62	0.08
μ_G^2						1.00	-0.08	-0.04
ρ_D^3							1.00	-0.14
ρ_{LS}^3								1.00

FIG. 13 (color online). The measured hadronic-mass moments $\langle m_X^k \rangle$, combined mass-and-energy moments $\langle n_X^k \rangle$, electron-energy moments $\langle E_\ell^k \rangle$, partial branching fractions B, and photon-energy moments $\langle E_\gamma^n \rangle$, as a function of the minimum lepton momentum $p_{\ell,\text{min}}^*$ and minimum photon energy $E_{\gamma,\text{min}}$ compared with the result of the simultaneous fit (solid line) to moments of the combined mass-and-energy spectrum, electron-energy moments, and photon-energy moments. The solid data points mark the measurements included in the fit. Moments of semileptonic decays $\bar{B} \to X_c \ell^- \bar{\nu}$ are marked by ($\bullet$). Photon-energy moments of Ref. [14] are marked by ($\blacksquare$), of Ref. [15] by ($\bullet$), and of Ref. [16] by ($\star$). Open data points are not used in the fit. The vertical bars indicate the experimental errors. The dashed lines correspond to the total fit uncertainty as obtained by converting the fit errors of each individual HQE parameter into an error for the individual moment.

TABLE VII.   Results of the simultaneous fit to moments of the combined mass-and-energy spectrum, electron-energy moments, and photon-energy moments. For $|V_{cb}|$ we account for an additional theoretical uncertainty of 1.4% from the uncertainty in the expansion of Γ_{SL}. Correlation coefficients for all parameters are summarized below the central values.

	$|V_{cb}| \times 10^3$	m_b [GeV/c^2]	m_c [GeV/c^2]	$\mathcal{B}$ [%]	μ_π^2 [GeV/c^2]	μ_G^2 [GeV/c^2]	ρ_D^3 [GeV/c^3]	ρ_{LS}^3 [GeV/c^3]
Results	41.91	4.566	1.101	10.637	0.452	0.304	0.190	-0.156
Δ_{exp}	0.48	0.034	0.045	0.166	0.023	0.047	0.013	0.079
Δ_{theo}	0.38	0.041	0.064	0.061	0.065	0.039	0.031	0.052
$\Delta_{\Gamma_{SL}}$	0.59							
Δ_{tot}	0.85	0.053	0.078	0.176	0.069	0.061	0.034	0.095
$|V_{cb}|$	1.00	-0.43	-0.24	0.74	0.41	-0.43	0.43	0.15
m_b		1.00	0.95	0.04	-0.58	0.20	-0.30	-0.27
m_c			1.00	0.11	-0.62	-0.05	-0.30	-0.19
$\mathcal{B}$				1.00	0.17	-0.09	0.16	-0.05
μ_π^2					1.00	0.01	0.68	0.14
μ_G^2						1.00	-0.05	-0.05
ρ_D^3							1.00	-0.08
ρ_{LS}^3								1.00

are the parameter uncertainties returned by the nominal fits. The rescaling factors range between 0.92 and 1.01.

1. Combined fit including hadronic-mass moments

A comparison of the fit including hadronic-mass moments with the measured moments is shown in Fig. 12. The moments $\langle m_X \rangle$ and $\langle m_X^3 \rangle$ as well as the combined mass-and-energy moments are not included in the fit and thus provide an unbiased comparison with the fitted HQE prediction. We find an overall good agreement, also indicated by $\chi^2 = 10.9$ for 28 degrees of freedom. Results for the SM and HQE parameters extracted from the fit are summarized in Table VI. We find $|V_{cb}| = (42.05 \pm 0.45 \pm 0.70) \times 10^{-3}$, $\mathcal{B}(\bar{B} \to X_c e^- \bar{\nu}) = (10.64 \pm 0.17 \pm 0.06)\%$, $m_b = (4.549 \pm 0.031 \pm 0.038)$ GeV/c^2, and $m_c = (1.077 \pm 0.041 \pm 0.062)$ GeV/c^2, where the errors correspond to experimental and theoretical uncertainties, respectively. The fitted quark masses have a large correlation of 95% resulting in a more precise determination of the quark mass difference, $m_b - m_c = (3.472 \pm 0.032)$ GeV/c^2, where the error is the total uncertainty. We translate the quark masses which were extracted in the kinetic scheme into the $\overline{\mathrm{MS}}$ scheme using calculations up to $\mathcal{O}(\alpha_s^2)$ accuracy [11]. The translation yields $\bar{m}_b(\bar{m}_b) = (4.186 \pm 0.044 \pm 0.015)$ GeV/c^2 and $\bar{m}_c(\bar{m}_c) = (1.196 \pm 0.059 \pm 0.050)$ GeV/c^2, where the first uncertainty is a translation of the uncertainty obtained in the kinetic scheme and the second corresponds to an estimate for the uncertainty of the transformation itself.

2. Combined fit including combined mass-and-energy moments

Figure 13 shows a comparison of the measured moments and the fit including the measured combined mass-and-energy moments. We find an overall good agreement

with $\chi^2 = 8.2$ for 28 degrees of freedom. The fit yields predictions of the hadronic-mass moments that are in good agreement with the measurement. Numerical results of the fit are summarized in Table VII. We find $|V_{cb}| = (41.91 \pm 0.48 \pm 0.70) \times 10^{-3}$, $\mathcal{B}(\bar{B} \to X_c e^- \bar{\nu}) = (10.64 \pm 0.17 \pm 0.06)\%$, $m_b = (4.566 \pm 0.034 \pm 0.041)$ GeV/c^2, and $m_c = (1.101 \pm 0.045 \pm 0.064)$ GeV/c^2, where the errors correspond to experimental and theoretical uncertainties, respectively. The two masses are correlated with 95%. Their difference is $m_b - m_c = (3.465 \pm 0.032)$ GeV/c^2, where the stated uncertainty corresponds to the total uncertainty. The extracted quark masses translate into the $\overline{\mathrm{MS}}$ scheme using [11] as $\bar{m}_b(\bar{m}_b) = (4.201 \pm 0.047 \pm 0.015)$ GeV/c^2 and $\bar{m}_c(\bar{m}_c) = (1.215 \pm 0.062 \pm 0.050)$ GeV/c^2, where the first uncertainty is a translation of the uncertainty obtained in the kinetic scheme and the second corresponds to an estimate for the uncertainty of the transformation itself.

3. Comparison of results

Comparing the result of the fit that includes moments of the n_X^2 distribution with that including hadronic-mass moments instead, we find good agreement of all fit parameters and their uncertainties. The differences between the fit values are 0.2 σ for $|V_{cb}|$, 0.3 σ for m_b, and 0.3 σ for m_c. The uncertainties of all fit parameters in both fits agree within 8%.

Figure 14 shows $\Delta\chi^2 = 1$ contours of both fits in the $(m_b, |V_{cb}|)$ and (m_b, μ_π^2) planes. We find an almost identical precision for the fit values of $|V_{cb}|$, m_b, and μ_π^2. In the Figure, we also show the results of two fits with reduced sets of input measurements. To illustrate the influence of the photon-energy measurements, a fit with only hadronic-mass and lepton-energy moments is performed. For further comparison we also perform a fit with only hadronic-mass moments and partial branching fractions. The fits with
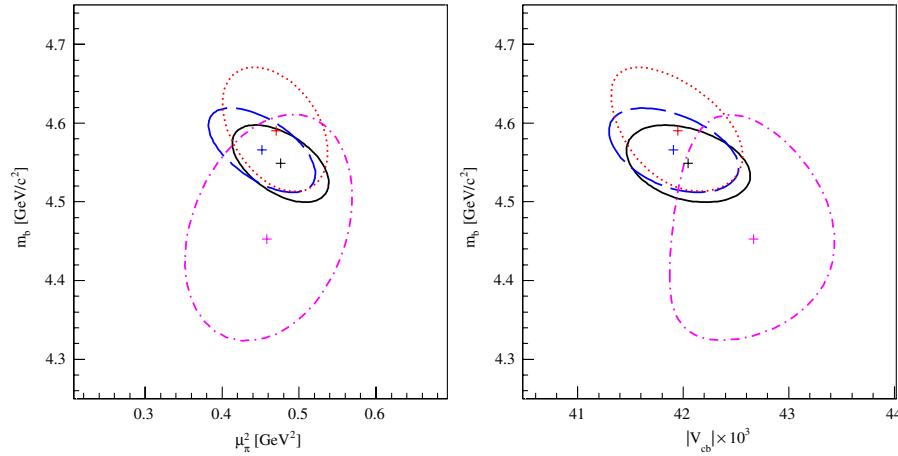
FIG. 14 (color online). $\Delta\chi^2 = 1$ contours for different fits in the $(m_b, |V_{cb}|)$ and (m_b, μ_π^2) planes. We compare the results of the two fits including the full sets of measured moments, one including hadronic-mass moments (black line) and one including moments of the n_X^2 distribution instead (blue dashed line), with a fit including only hadronic-mass and lepton-energy moments (red dotted line) and a fit including only hadronic-mass moments and partial branching-fraction measurements (magenta dashed-dotted line). We do not include the additional uncertainty of 1.4% due to the expansion of Γ_{SL} in the plotted values of $|V_{cb}|$.

reduced experimental input show a significantly reduced accuracy of the extracted parameters.

As our primary results we choose the values extracted from the fit with hadronic-mass moments since this fit has been used extensively before. Its results are in good agreement with earlier determinations [17,59], but their uncertainties are slightly larger because of the restrictions to *BABAR* data only.

The use of combined mass-and-energy moments n_X^2 does not lead to a more precise determination of the fundamental physics parameters $|V_{cb}|$, m_b, and m_c. However, the agreement of both fits confirms that higher-order corrections, which are needed for the expansion of the hadronic-mass moments but not for the n_X^2 moments, have been estimated correctly. A significant change in the uncertainties of the SM and HQE parameters would have indicated a too naive treatment of the corrections for the mass moments [57]. Consequently, the presented results have increased the confidence into the validity of error estimates that have to be made for a reliable determination of m_b, m_c, and $|V_{cb}|$.

ACKNOWLEDGMENTS

[1] N. Cabibbo, Phys. Rev. Lett. **10**, 531 (1963).

[2] M. Kobayashi and T. Maskawa, Prog. Theor. Phys. **49**, 652 (1973).

[3] Charge-conjugate processes are implied throughout this paper.

[4] S. E. Csorna *et al.* (CLEO Collaboration), Phys. Rev. D **70**, 032002 (2004).

[5] B. Aubert *et al.* (*BABAR* Collaboration), Phys. Rev. D **69**, 111103 (2004).

[6] D. Acosta *et al.* (CDF Collaboration), Phys. Rev. D **71**,

051103 (2005).

[7] J. Abdallah *et al.* (DELPHI Collaboration), Eur. Phys. J. C **45**, 35 (2006).

[8] C. Schwanda *et al.* (Belle Collaboration), Phys. Rev. D **75**, 032005 (2007).

[9] B. Aubert *et al.* (*BABAR* Collaboration), Phys. Rev. D **69**, 111104 (2004).

[10] P. Urquijo *et al.*, Phys. Rev. D **75**, 032001 (2007).

[11] D. Benson, I. I. Bigi, T. Mannel, and N. Uraltsev, Nucl. Phys. **B665**, 367 (2003).

[12] S. Chen *et al.* (CLEO Collaboration), Phys. Rev. Lett. **87**, 251807 (2001).

[13] P. Koppenburg *et al.* (Belle Collaboration), Phys. Rev. Lett. **93**, 061803 (2004).

[14] B. Aubert *et al.* (*BABAR* collaboration), Phys. Rev. D **72**, 052004 (2005).

[15] B. Aubert *et al.* (*BABAR* collaboration), Phys. Rev. Lett. **97**, 171803 (2006).

[16] B. Aubert *et al.* (*BABAR* collaboration), Phys. Rev. D **77**, 051103 (2008).

[17] O. Buchmüller and H. Flächer, Phys. Rev. D **73**, 073008 (2006).

[18] E. Barberio *et al.* (Heavy Flavor Averaging Group (HFAG)) (Summer 2007).

[19] C. Schwanda *et al.* (Belle Collaboration), Phys. Rev. D **78**, 032016 (2008).

[20] P. Gambino and N. Uraltsev, Eur. Phys. J. C **34**, 181 (2004).

[21] W.-M. Yao *et al.* (Particle Data Group (PDG)) (2007), URL http://pdg.lbl.gov.

[22] B. Aubert *et al.* (*BABAR* Collaboration), Nucl. Instrum. Methods Phys. Res., Sect. A **479**, 1 (2002).

[23] PEP-II: An Asymmetric *B* Factory. Conceptual Design Report, SLAC Report No. SLAC-R-418 1993.

[24] D. J. Lange, Nucl. Instrum. Methods Phys. Res., Sect. A **462**, 152 (2001).

[25] S. Agostinelli *et al.* (GEANT Collaboration), Nucl. Instrum. Methods Phys. Res., Sect. A **506**, 250 (2003).

[26] E. Richter-Was, Phys. Lett. B **303**, 163 (1993).

[27] E. Barberio *et al.* (Heavy Flavor Averaging Group (HFAG)) (Winter 2006), arXiv:hep-ex/0603003; URL http://www.slac.stanford.edu/xorg/hfag.

[28] B. Aubert *et al.* (*BABAR* collaboration), Phys. Rev. D **76**, 051101 (2007).

[29] B. Aubert *et al.* (*BABAR* collaboration), Phys. Rev. Lett. **100**, 231803 (2008).

[30] B. Aubert *et al.* (*BABAR* collaboration), Phys. Rev. Lett. **103**, 051803 (2009).

[31] B. Aubert *et al.* (*BABAR* collaboration), Phys. Rev. D **73**, 012006 (2006).

[32] I. I. Bigi, M. A. Shifman, and N. Uraltsev, Annu. Rev. Nucl. Part. Sci. **47**, 591 (1997).

[33] I. Caprini, L. Lellouch, and M. Neubert, Nucl. Phys. **B530**, 153 (1998).

[34] B. Grinstein and Z. Ligeti, Phys. Lett. B **526**, 345 (2002).

[35] J. E. Duboscq *et al.* (CLEO Collaboration), Phys. Rev. Lett. **76**, 3898 (1996).

[36] D. Scora and N. Isgur, Phys. Rev. D **52**, 2783 (1995).

[37] J. L. Goity and W. Roberts, Phys. Rev. D **51**, 3459 (1995).

[38] B. Aubert *et al.* (*BABAR* Collaboration), Phys. Rev. Lett. **92**, 071802 (2004).

[39] H. Albrecht *et al.* (ARGUS Collaboration), Phys. Lett. B **185**, 218 (1987).

[40] T. Skwarnicki (Crystal Ball Collaboration), DESY Report No. DESY F31-86-02 1986.

[41] B. Aubert *et al.* (*BABAR* collaboration), Phys. Rev. D **75**, 072002 (2007).

[42] N. E. Adam *et al.* (CLEO Collaboration), Phys. Rev. Lett. **97**, 251801 (2006).

[43] See supplementary material at http://link.aps.org/supplemental/10.1103/PhysRevD.81.032003 for the correlation matrices of lepton energy and hadronic moments.

[44] M. Voloshin and M. Shifman, Sov. J. Nucl. Phys. **41**, 120 (1985).

[45] J. Chay, H. Georgi, and B. Grinstein, Phys. Lett. B **247**, 399 (1990).

[46] I. I. Y. Bigi and N. G. Uraltsev, Phys. Lett. B **280**, 271 (1992).

[47] I. I. Bigi, N. Uraltsev, and A. I. Vainshtein, Phys. Lett. B **293** (1992).

[48] I. I. Bigi, M. Shifman, N. G. Uraltsev, and A. Vainshtein, Phys. Rev. Lett. **71**, 496 (1993).

[49] B. Blok, L. Koyrakh, M. Shifman, and A. I. Vainshtein, Phys. Rev. D **49**, 3356 (1994).

[50] A. V. Manohar and M. B. Wise, Phys. Rev. D **49**, 1310 (1994).

[51] M. Gremm and A. Kapustin, Phys. Rev. D **55**, 6924 (1997).

[52] D. Benson, I. I. Bigi, and N. Uraltsev, Nucl. Phys. **B710**, 371 (2005).

[53] V. Aquila, P. Gambino, G. Ridolfi, and N. Uraltsev, Nucl. Phys. **B719**, 77 (2005).

[54] N. Uraltsev, Int. J. Mod. Phys. A **20**, 2099 (2005).

[55] I. I. Bigi, N. Uraltsev, and R. Zwicky, Eur. Phys. J. C **50**, 539 (2007).

[56] I. Bigi, M. Shifman, N. Uraltsev, and A. Vainshtein, Phys. Rev. D **56**, 4017 (1997).

[57] N. Uraltsev (private communication).

[58] B. Aubert *et al.* (*BABAR* collaboration), Phys. Rev. Lett. **93**, 011803 (2004).

[59] C. W. Bauer *et al.*, Phys. Rev. D **70**, 094017 (2004).